INFLUENCE OF BACKUP BEARINGS AND SUPPORT STRUCTURE DYNAMICS ON THE BEHAVIOR OF ROTORS WITH ACTIVE SUPPORTS

Annual Status Report for Research Grant Number NAG3-1507

submitted to:

National Aeronautics and Space Administration
Lewis Research Center
Cleveland, Ohio 44135

by

George T. Flowers, Ph.D
Assistant Professor

Department of Mechanical Engineering
Auburn University
Auburn University, AL 36849-5341
Phone: (334) 844-3330

June, 1995

INFLUENCE OF BACKUP BEARINGS AND SUPPORT STRUCTURE DYNAMICS ON THE BEHAVIOR OF ROTORS WITH ACTIVE SUPPORTS

Annual Status Report for Research Grant Number NAG3-1507

submitted to:

National Aeronautics and Space Administration
Lewis Research Center
Cleveland, Ohio 44135

by

George T. Flowers, Ph.D
Assistant Professor

Department of Mechanical Engineering
Auburn University
Auburn University, AL 36849-5341
Phone: (334) 844-3330

June, 1995

Progress to Date

This report documents the progress that has been made in the proposed research work since the first annual report. The basic goals for year two have been completed. Specific accomplishments for the past year are itemized below.

1. A paper has been presented that documents the work using the T-501 engine model. The paper was presented at the *Symposium on Nonlinear and Stochastic Dynamics*, held at the *1994 ASME Winter Annual Meeting*, November 13-18, 1994, Chicago, Illinois. The paper has also been submitted to the *ASME Journal of Vibration and Acoustics*. A copy of the paper is included in the Appendix.

2. A paper that discusses some of the work using the T-501 engine model has been presented at the *First Industry/University Symposium on High Speed Civil Transport Vehicles*, December 4-6, 1994, Greensboro, North Carolina. A copy of the paper is included in the Appendix.

3. Development of the experimental facilities has continued. This includes a new design for the magnetic bearing and the inclusion of housing dynamics in an additional test rig.

4. A paper that documents an experimental/simulation study of auxiliary bearing rotordynamics has been presented at the *40th ASME International Gas Turbine and Aeroengine Conference*, June 5-8, 1995, Houston, Texas. A copy of the paper is included in the Appendix.

5. A paper that describes a rotordynamical model for a magnetic bearing supported rotor system, including auxiliary bearing effects has been written and submitted to the *ASME 15th Biennial Conference on Vibration and Sound*, to be held in Boston, Massachusetts, Sept. 17-21, 1995. A copy of the paper is included in the Appendix.

6. A finite element model for a foil bearing has been developed. Rotordynamical studies of a rotor supported by foil bearings is currently underway. This includes a study of the influence of nonlinear effects arising from foil bearings on rotordynamic behavior.

7. Additional studies of rotor/bearing/housing dynamics are currently being performed with the experimental rig and simulation models.

8. The effects of sideloading on auxiliary bearing rotordynamics is being studied using the magnetic bearing supported rotor model.

9. Two students affiliated with this project have graduated with M.S. degrees - April M. Free and James L. Lawen, Jr.

Bibliography

1. Flowers, G.T., Xie, Huajun, and Lawrence, C. "Steady-State Dynamic Behavior of an Auxiliary Bearing Supported Rotor System," presented at the *Symposium on Nonlinear and Stochastic Dynamics*, held at the *1994 ASME Winter Annual Meeting*, November 13-18, 1994, Chicago, Illinois; also submitted to the *ASME Journal of Vibration and Acoustics*.

2. Flowers, G.T., Xie, H., and Sinha, S.C., " Dynamic Behavior of a Magnetic Bearing Supported Jet Engine Rotor with Auxiliary Bearings," presented at the *First Industry/University Symposium on High Speed Civil Transport Vehicles*, Greensboro, North Carolina, December 4-6, 1994.

3. Lawen, James L., Jr., and Flowers, George T.,"Synchronous Dynamics of a Coupled Shaft/Bearing/Housing System With Auxiliary Support From a Clearance Bearing: Analysis and Experiment," presented at the *40th ASME International Gas Turbine and Aeroengine Conference*, June 5-8, 1995; also accepted for publication in the *ASME Journal of Engineering for Gas Turbines and Power*.

4. Free, A., Flowers, George T., and Trent, Victor S., "Dynamic Modelling of a Magnetic Bearing Rotor System Including Auxiliary Bearings," to be presented at the *ASME 15th Biennial Conference on Vibration and Noise*, Sept. 17-21, 1995, Boston, Massachusetts; also, submitted to the *Journal of Vibration and Control*.

Appendix

Presented at: ASME International Mechanical Engineering Congress and Exposition
'Symposium on Nonlinear and Stochastic Dynamics'
Chicago, Illinois
November 13-18, 1994

STEADY-STATE DYNAMIC BEHAVIOR OF AN AUXILIARY BEARING SUPPORTED ROTOR SYSTEM

Huajun Xie and George T. Flowers

Department of Mechanical Engineering
Auburn University
Auburn, Alabama

Charles Lawrence

NASA Lewis Research Center
Cleveland, Ohio

ABSTRACT

This paper investigates the steady-state responses of a rotor system supported by auxiliary bearings in which there is a clearance between the rotor and the inner race of the bearing. A simulation model based upon the rotor of a production jet engine is developed and its steady-state behavior is explored over a wide range of operating conditions for various parametric configurations. Specifically, the influence of rotor imbalance, support stiffness and damping is studied. It is found that imbalance may change the rotor responses dramatically in terms of frequency contents at certain operating speeds. Subharmonic responses of 2nd order through 10th order are all observed except the 9th order. Chaotic phenomenon is also observed. Jump phenomena (or double-valued responses) of both hard-spring type and soft-spring type are shown to occur at low operating speeds for systems with low auxiliary bearing damping or large clearance even with relatively small imbalance. The effect of friction between the shaft and the inner race of the bearing is also discussed.

NOMENCLATURE

C_B = auxiliary bearing support damping, lb.s^2/in.
$C_{B\psi}$ = auxiliary bearing torsional damping, lb.in.s
F_n = normal force, lb
F_t = friction force, lb
$\mathbf{F}_X$ = external force vector acting on the rotor in X direction
$\mathbf{F}_Y$ = external force vector acting on the rotor in Y direction
$\mathbf{I}_a$ = rotor inertia matrix
J_B = moment of inertia of auxiliary bearing, lb.in.s^2
K_B = auxiliary bearing support stiffness, lb/in.
K_C = contact stiffness, lb/in.
M_B = auxiliary bearing mass, lb.s^2/in.
M_k = mass of kth rotor element, lb.s^2/in.
N = total number of modes considered
$NB1$ = node number at auxiliary bearing #1
$NB2$ = node number at auxiliary bearing #2
$\mathbf{Q}_X$ = rotor modal coordinate vector in X direction
$\mathbf{Q}_Y$ = rotor modal coordinate vector in Y direction
R_B = radius of auxiliary bearing bore, in.
R_m = radius of auxiliary bearing pitch, in.
R_R = radius of rotor journal, in.
$\mathbf{X}_R$ = rotor physical coordinate vector in X direction
$\mathbf{Y}_R$ = rotor physical coordinate vector in Y direction
e = rotor imbalance eccentricity, in.
g = gravitational acceleration, in./s^2
t = time, s
Δ = deformation at the contact point, in.
$\mathbf{\Gamma} = \mathbf{\Psi}^T \mathbf{I}_a \mathbf{\Psi}$
$\mathbf{\Psi}$ = rotor free-free modal rotation matrix
Ω = rotor operating speed, rad/s
$\mathbf{\Phi}$ = rotor free-free modal displacement matrix
$\delta = R_B - R_R$, auxiliary bearing clearance, in.
μ = dynamic friction coefficient
μ_ψ = rolling friction coefficient
ψ_B = angular displacement of auxiliary bearing inner-race
ζ = modal damping coefficient

INTRODUCTION

One of the most innovative developments in the turbomachinery field involves the use of active magnetic bearings (AMB) for rotor support. This technology provides the potential for significant improvements in the dynamic behavior of rotor systems, allowing for loading, eccentricity, shaft position and vibration to be continuously monitored and controlled. In order to protect the soft iron cores of the magnetic bearings and to provide rotor support in the event of failure of the bearing or during an overload situation, backup (or auxiliary) bearings, with a clearance between the rotor and the inner race of the bearing, are usually included in the rotor design. This clearance introduces a nonlinear dynamical feature which may significantly impact the behavior of the rotor.

Magnetic bearing systems appear to provide particularly great promise for use in aerospace applications. There are active programs at many of the major jet engine manufacturers to develop engines supported by magnetic bearings. Safety is a major concerns in any aeronautical design. Toward this end, it is desirable to design the rotor system to take maximum advantage of the backup bearings and use them as true auxiliary bearings to provide support during critical situations in a safe and consistent manner. An important concern in this regard is the dynamic behavior of the rotor when it comes into contact with the auxiliary bearing. If safe and effective operation of the engine is to be ensured during these periods, it is essential that designers have a very good understanding of the steady-state dynamics of rotor systems with clearance effects.

There are a number of studies in the literature concerned with the dynamics of rotors with clearance effects. Yamamoto (1954) conducted a systematic study of rotor responses involving bearing clearance effects. Black (1968) studied the rotor/stator interaction with a clearance. He concluded that rotor/stator interactions may occur in a variety of forms and circumstances, including jump phenomena. Ehrich (1966) reported the first identification of a second order subharmonic vibration phenomenon in a rotor system associated with bearing clearance (1966). Bently (1974) published experimental observations of second and third order subharmonic vibration in a rotor system. Later, Muszynska (1984) cited the occurrence of second, third, and fourth order subharmonic responses in a rotor rubbing case and Ehrich (1988 and 1991) observed eighth and ninth order subharmonic vibration as well as chaotic vibration in a high speed turbomachine. Childs (1979 and 1982) published two papers to explain the mechanism for the second and third order subharmonic responses noted above. He stated, with great insight, that " motion due to nonsymmetric clearance effects is a fractional-frequency phenomenon."

While those studies have greatly enhanced the understanding of clearance effects on rotor dynamics, a more detailed understanding of the dynamical behavior of such systems is needed. The perspective of much of this earlier work is that the clearance exists as a result of manufacturing error or misfitting. That is, it is due to an abnormal situation. However, in a rotor system fitted with magnetic bearings and auxiliary bearings, the clearance becomes a design parameter rather than an irregularity. From this point of view, it is important to develop a detailed quantitative understanding of the dynamic responses that are to be expected. Such knowledge will provide guidelines for the selection of auxiliary bearing parameters.

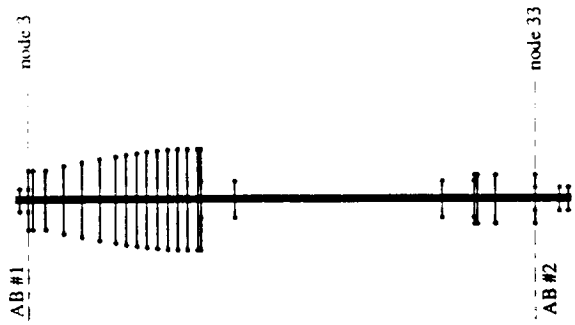

FIG. 1 DIAGRAM OF THE FEM ROTOR MODEL

It seems that there have been little work to date that is specifically concerned with auxiliary bearings in magnetic bearing supported rotor systems. Two papers that are directly related to research on auxiliary bearings were both focused on transient responses. Gelin et al. (1990) studied the transient dynamic behavior of rotors on auxiliary bearings during the coast down. Ishii and Kirk (1991) investigated the transient responses of a flexible rotor during the rotor drop after the magnetic bearings become inactive. In both papers, idealized rotor models are used and it is assumed that once the magnetic bearings fail, the torque is cut off and consequently the rotor speed approaches zero.

In this paper, simulation results are presented for a complex rotor system supported by auxiliary bearings with clearance at each end of the rotor. This work is specifically concerned with systems in which the clearances are quite small (on the order of a few mils), which is appropriate for jet engine applications in which the backup bearing is acting to provide rotor support on a consistent basis. The influence of rotor imbalance, support stiffness and support damping are investigated using direct numerical integration of the governing equations of motion and the harmonic balance method. Some insights are obtained with regard to the frequency and amplitude behavior of the steady-state vibration of such a system.

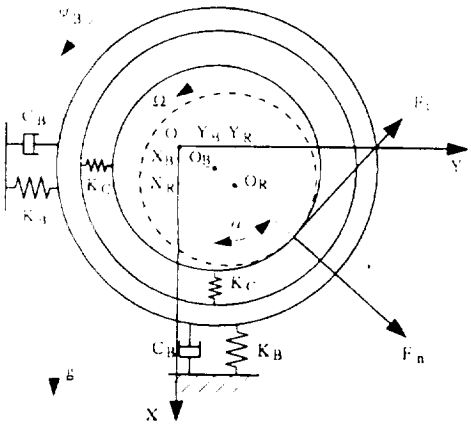

FIG. 2 AUXILIARY BEARING MODEL

SIMULATION MODEL

The rotor is modelled using free–free normal mode shapes and natural frequencies obtained through finite element analysis. The model data is representative for the rotor of a jet engine. Fig. 1 shows a schematic diagram of the FEM rotor model. Parametric information about the model is listed in Table 1. The torsional motion of the shaft is not considered in this paper. Using state space representation and modal coordinates, the equations of motion for the rotor are expressed as

$$\ddot{\mathbf{Q}}_X + 2\zeta\omega_n\dot{\mathbf{Q}}_X + \Omega\mathbf{\Gamma}\dot{\mathbf{Q}}_Y + \omega_n^2\mathbf{Q}_X + 2\Omega\zeta\omega_n\mathbf{Q}_Y = \mathbf{\Phi}^T\mathbf{F}_X, \quad (1.a)$$

$$\ddot{\mathbf{Q}}_Y + 2\zeta\omega_n\dot{\mathbf{Q}}_Y - \Omega\mathbf{\Gamma}\dot{\mathbf{Q}}_X + \omega_n^2\mathbf{Q}_Y - 2\Omega\zeta\omega_n\mathbf{Q}_X = \mathbf{\Phi}^T\mathbf{F}_Y, \quad (1.b)$$

where

$$\mathbf{F}_X = \{F_{X1}, F_{X2}, \ldots, F_{Xm}\}^{-1},$$
$$\mathbf{F}_Y = \{F_{Y1}, F_{Y2}, \ldots, F_{Ym}\}^{-1},$$
$$\mathbf{Q}_X = \mathbf{\Phi}^{-1}\mathbf{X}_R,$$
$$\mathbf{Q}_Y = \mathbf{\Phi}^{-1}\mathbf{Y}_R,$$

with

$$\mathbf{X}_R = \{X_{R1}, X_{R2}, \ldots, X_{Rm}\}^{-1},$$
$$\mathbf{Y}_R = \{Y_{R1}, Y_{R2}, \ldots, Y_{Rm}\}^{-1}.$$

(m = total number of nodes)

The physical displacements of the rotor at the two auxiliary bearing locations can be obtained using the following coordinate transformation:

$$X_{Rk} = \sum_{i=1}^{N} \Phi_{ik} Q_{Xi}, \qquad Y_{Rk} = \sum_{i=1}^{N} \Phi_{ik} Q_{Yi}, \qquad (k = NB1, NB2)$$

The equations of motion for the auxiliary bearings are derived using the model shown in Fig. 2

$$M_{Bk}\ddot{X}_{Bk} + C_{Bk}\dot{X}_{Bk} + K_{Bk}X_{Bk} = F_{nk}\cos\alpha_k - F_{tk}\sin\alpha_k + M_{Bk}g, \quad (2.a)$$

$$M_{Bk}\ddot{Y}_{Bk} + C_{Bk}\dot{Y}_{Bk} + K_{Bk}Y_{Bk} = F_{nk}\sin\alpha_k + F_{tk}\cos\alpha_k, \quad (2.b)$$

$$J_{Bk}\ddot{\psi}_{Bk} + C_{B\psi k}\dot{\psi}_{Bk} = F_{tk}R_{Bk} - \mu_\psi F_{nk}R_{mk}, \quad (2.c)$$

where

$$\alpha_k = tan^{-1}\frac{Y_{Rk} - Y_{Bk}}{X_{Rk} - X_{Bk}}. \qquad (k = NB1, NB2)$$

At this point, the rotor and the back-up bearings appear to be uncoupled. However, the force vectors $\mathbf{F}_X$ and $\mathbf{F}_Y$ on the right hand sides of equations (1) are partially due to rotor/auxiliary bearing interaction. In fact, we have

$$F_{Xk} = -F_{nk}\cos\alpha_k + F_{tk}\sin\alpha_k + M_k g + M_k e\Omega^2\cos(\Omega t),$$
$$F_{Yk} = -F_{nk}\sin\alpha_k - F_{tk}\cos\alpha_k + M_k e\Omega^2\sin(\Omega t).$$

The rotor/bearing interaction is represented with the normal force F_{nk}

$$F_{nk} = \begin{cases} K_C\delta_k, & \Delta_k < 0, \\ 0, & \Delta_k \geq 0, \end{cases} \quad (3.a)$$

where

$$\Delta_k = (X_{Rk} - X_{Bk})\cos\alpha_k + (Y_{Rk} - Y_{Bk})\sin\alpha_k - \delta_k$$

and the Coulomb friction force F_{tk}. As long as there exists slip at the contact point, the friction force obeys

$$F_{tk} = \mu F_{nk}. \quad (3.b)$$

However, when there is no slip at the contact point, the friction forces are solved from equations (1) and (2) using

the kinematic constraint that the circumferential velocities of the rotor and the inner-race of the back-up bearing at the contact point equal to each other. At the same time, if this solved friction force exceeds the maximum static friction force ($= \mu_s F_{nk}$), equation (3.b) applys again.

DISCUSSION OF RESULTS

The rotor is modeled with 34 stations (as shown in Fig. 1) and the first four modes (two rigid body and two flexible modes) are included in the simulation model. The two auxiliary bearings are located at nodes 3 and 33, respectively. This arrangement is taken to represent one of the most technically feasible configurations in that it greatly simplifies bearing maintenance. It is assumed that the two auxiliary bearings are identical in terms of stiffness, damping and friction characteristics. Some nominal system parameters used for the simulation study are K_C=2.855e+6, ξ=0.03, R_{mk}=1.1 R_{Bk}, μ_s=0.5 and μ_ψ=0.002. To avoid excessive cluttering of plots, all the results that are presented in this paper correspond to node 3, the location of bearing #1.

Since the total system which includes two bearings and associated friction forces as well as the inner–race motions is rather complicated and requires considerable amount of computer time for the solutions to converge, the friction effect is examined first to see if the model can be further simplified. It turns out that the steady–state results obtained with and without friction are virtually identical. Even the differences in transient responses are quite small, as can be seen in Fig. 3(a) and 3(b). The only remarkable effect is on the transient responses of the inner-race as shown in Fig. 3(c). This observation is confirmed by numerous runs using different system parameters and rotor speeds. The lack of significance of friction may be attributed to several factors. First, the inertia of the inner-race is quite small in comparison to the rotor mass, so vibration of the bearing has little influence on the rotor vibration. Second, ball bearings exhibit quite negligible torsional resistance under normal conditions. As a result, the terms that are related to the friction forces and the rotational motion of the inner race are not included in the simulations that are discussed in the following paragraphs.

The steady–state response characteristics of the system are obtained through numerical integration of the simplified version of governing equations (1) and (2). Near–zero initial conditions are used, simulating situations where the AMBs are functioning properly prior to a system failure. Multiple solutions with other initial conditions are not sought at present.

It is well known from linear analyses that imbalance greatly affects the steady state vibration amplitudes of a rotor system. However, it is observed from the current work that imbalance may also influence frequency content of the rotor responses quite dramatically at certain operating speeds. A typical case with such an imbalance effect is shown in Figs. 4 and 5, where orbits and corresponding frequency spectra of the rotor for different values of imbalance at the speed of $\Omega = 1000$ are plotted. For this particular case, there exist eight ranges of imbalance values that result in eight different types of rotor responses.

For $e \leq 0.0009$, the rotor rotates near the bottom of auxiliary bearings and the responses are predominantly synchronous (Figs. 4(a)-4(b) and 5(a)-5(b)). As imbalance increases, the 2Ω superharmonic component approaches the magnitude order of the synchronous component (Figs. 4(b) and 5(b)). However, the responses are of small amplitude. For $0.0010 \leq e \leq 0.0013$, the responses are dominated by $\Omega/2$ subharmonic components (Figs. 4(c) and 5(c)). In other words, the amplitude of $\Omega/2$ component is greater than that of the synchronous. For $0.0014 \leq e \leq 0.0016$, the $\Omega/2$ subharmonics disappear and the $\Omega/3$ subharmonics become dominant (Figs. 4(d) and 5(d)). So far, the overall amplitude of the responses are not large, the rotor just bounces near the bottom of the auxiliary bearings. For $0.0017 \leq e \leq 0.0027$, the orbits become chaotic-looking (Fig. 4(e)) and the spectrum contains a lot of noise (Fig. 5(e)). In this range of imbalance, the rotor changes from bouncing near the bottom to bouncing around the full clearance of the bearing as imbalance increases. In the middle of this transition range, true chaos is observed. The Poincare map shown in Fig. 6(a) and the frequency spectrum shown in Fig. 6(b) demonstrate that the response has all the characteristics of a chaotic phenomenon. It should be noted that even though the orbits are chaotic looking, the amplitudes are not the largest among all the cases for this particular parametric configuration. For $0.0028 \leq e \leq 0.0034$, the orbits orbits are no longer chaotic–looking (Fig. 4(f)). The spectrum shows they are $\Omega/5$ subharmonic responses (Fig. 5(f)). Notice the amplitudes are the largest for this parametric configuration. For $e = 0.0035$, the amplitude suddenly becomes smaller even though the imbalance has become larger (Fig. 4(g)). And the rotor bounces near the bottom of the auxiliary bearings again. The frequency spectrum shows it is $\Omega/8$ subharmonic response (Fig. 5(g)). For $0.0036 \leq e \leq 0.0042$, the orbits become chaotic-looking again (Fig. 4(h)). But the frequency spectra are very similar to the subharmonic cases (Fig. 5(h)), only with some discrete noise. Finally, for $e \geq 0.0043$, the responses become predominantly synchronous again (Figs. 4(i)-4(j) and 5(i)-5(j)). But this time as imbalance increases, the 2Ω superharmonic component become smaller and smaller (Figs. 4(j) and 5(j)).

Examining all the orbits in terms of amplitudes as imbalance increases, we can see the characteristics of a jump–type phenomenon (Cunningham, 1958). The jump–down takes place around $0.0034 < e < 0035$ where the rotor jumps

from full-clearance bouncing to near-bottom bouncing. Further investigation is needed to better understand this type of change.

Imbalance responses at some other operating speeds and for other parametric configurations exhibit similar changes as imbalance varies, though the imbalance ranges and corresponding response types may not be as well defined as in the above cases. In fact, subharmonic responses from $\Omega/2$ through $\Omega/10$ are all observed except $\Omega/9$ as shown in Figs. 7. Surprisingly, those subharmonics are not directly related to the system's natural frequencies as were the cases with other researchers' findings (such as Ehrich, 1988). Moreover, several types of subharmonic responses may occur at a single operating speed. It should be noted that Chen et al. (1993) also reported occurrence of three stable subharmonic responses at a single rotor speed in a SFD supported rotor system but did not provide any explanation for their findings. In their case, even the imbalance did not vary. Apparently, further research is needed to find a mechanism to explain this multi-subharmonic vibration phenomenon. On the other hand, it should be pointed out that these subharmonic responses are not typical cases. While some of them are observed to exist within a certain range of parameters, the majority of them occur only for some specific parametric configurations.

Due to space limitations, results for other parametric configurations are not systematically plotted. A general summation of the observations is presented instead. A common feature among all the responses is that for very small imbalance, the responses are always synchronous. The imbalance range that result in synchronous dominated responses depend on several system parameters. For small back-up bearing stiffness (such as K_B = 0.213e+6) and normal damping (C_B = 157.0), the responses are almost always synchronous. Only $\Omega/2$ subharmonic are observed at a few operating speeds with a very narrow range of imbalance. It should be noted that even though a lower K_B may leads to a better system response, it may also fail to protect the magnetic bearings due to the fact that it could result in a larger rotor orbit-center offset. However, the dramatic response changes discussed above may occur again if the damping becomes small (such as C_B = 57.0) even though the stiffness still remains small. On the other hand, increasing the damping C_B alone may not be able to eliminate those dramatic changes. It is observed that those changes can still occur for C_B being as large as 700.0. Reducing the size of clearance δ may not eliminate the response changes at certain speeds. But it can narrow the operating speed range where those changes occur. For example, response changes are eliminated for $\Omega \geq 1500$ when δ is reduced from 0.002 to 0.001 with all other parameters remaining the same, but response changes still occur for $\Omega \leq 1400$.

It is obvious that rotor responses involving nonsymmetric bearing clearance effect are very complex problems and numerical integration alone is not a sufficient tool to obtain a global picture of the system responses. The harmonic balance method is then used for the investigation of global system behavior. However, it is only attempted for situations with very small imbalance values. In addition, only the 1Ω harmonic is considered. The complex frequency contents associated with medium and large imbalance values makes it a formidable task to apply the harmonic balance method for other cases. Nevertheless, some useful information can be drawn from these results. After all, an adequately balanced rotor system should have very small imbalance under normal conditions.

Fig. 8(a) shows that nonsymmetric clearance effect is equivalent to asymmetric stiffness effect with regards to critical speeds. The clearance actually splits the first critical speed into two pseudo-critical speeds. In the X direction, the gravity force tends to keep the rotor in contact with the bearing at low operating speed. Thus, the apparent stiffness is almost the same as K_B and the pseudo-critical speed is nearly the same as the critical speed for the linear case ($\delta = 0$). But in the Y direction, the clearance results in a lower apparent stiffness and, consequently, an additional lower-value pseudo-critical speed. It is seen that several higher order additional pseudo-critical speeds are created in the operating speed range in addition to the 1st additional pseudo-critical speed. It is noted that the response in the X direction also departs from the linear case at high operating speed. This is because the imbalance force becomes dominant at high rotor speed which in turn makes the gravity force less significant and the clearance effect more important. Fig. 8(b) shows that changing the auxiliary bearing stiffness has little effect on the pseudo-critical speeds of the system. However, for a larger value of imbalance, a higher K_B does leads to a greater tendency of double-valued responses. In each direction, for either a stiffness increase or an imbalance increase, the 1st pseudo-critical peak tend to become a hard-spring type jump and the 2nd one tend to develop into a soft-spring type jump, with the tendency decreasing as the pseudo-critical's order increases.

Fig. 9(a) shows double-valued responses in the Y direction for four different values of clearance. It is seen that a larger clearance results in wider rotor speed range of double-valued responses. It is also observed that as clearance increases, the apparent stiffness decreases and the first pseudo-critical speed shifts to a lower value. Fig. 9(b) shows the double-valued responses in the X direction. Even though the jumps themselves are smaller in magnitude, they are more obvious in trend. Notice how little the change is for the first pseudo-

critical speed in the X direction.

Fig. 10(a) shows the influence of auxiliary bearing damping on the double-valued responses in the Y direction. It is observed that the damping has to be quite large to eliminate the double-valued responses associated with the first pseudo-critical speed. Fig. 10(b) shows the influence of C_B on the double-valued responses in the X direction. In both figures, it should be noted that as C_B decreases, the second pseudo-critical speed peak will develop into a soft-spring type jump and the third pseudo-critical speed peak will evolve into a hard-spring type jump.

The system behaviors for higher operating speed range are not shown in Figs. (9) and (10) so that the jump phenomena can be more clearly illustrated. It is also because that the system's responses at high operating speed range with the same parameters are more or less regular, in other words, mainly amplitude changes.

CONCLUSIONS

As a summary of the results discussed above, the following conclusions can be drawn:

1. Imbalance may change the rotor responses dramatically in terms of frequency contents at certain operating speeds, especially under conditions of large clearance, high bearing stiffness and low bearing damping. With imbalance changing, as many as eight different types of responses may occur for a particular parametric configuration at a single operating speed.
2. Subharmonic responses of second order through tenth order are all observed except for the ninth order case. However, the majority of them are not typical cases, and were observed only for quite particular parametric configurations.
3. Chaotic phenomenon is observed to occur occasionally. However, the amplitudes associated with such motion are not among the largest.
4. Nonsymmetric clearance effects influence the critical speeds in a manner similar to asymmetric stiffness effects.
5. Double-valued responses in the form of both hard-spring type jump and soft-spring type jump are observed to be possible at low operating speeds with low auxiliary bearing damping or high imbalance. With large clearances or high bearing stiffness, the jump phenomenon may occur for even relatively small imbalances.
6. The effect of friction between the shaft and the inner race of a rolling element auxiliary bearing on the dynamics of the rotor is quite small and can reasonably be neglected for steady-state analyses.

ACKNOWLEDGEMENT

The authors would like to express their gratitude to S. Klusman of Allison Gas Turbines, Inc. for many helpful discussions and practical advice.

This work was supported by NASA under Grant No. NAG3-1507. The Government has certain rights in this material.

REFERENCES

Bently, D. E., 1974, "Forced Subrotative Speed Dynamic Action of Rotating Machinery," ASME Paper No. 74-PET-16.

Black, H. F., 1968, "Interaction of a Whirling Rotor With a Vibrating Stator Across a Clearance Annulus," *Journal of Engineering Sci ence*, Vol. 10, No. 1, pp. 1-12.

Chen, P. Y. P, Hahn, E. J., and Wang, G. Y., 1993, "Subharmonic Oscillations in Squeeze Film Damped Rotor Bearing Systems Without Centralizing Springs," ASME Paper 93-GT-428.

Childs, D. W., 1979, "Rub-Induced Parametric Excitation in Rotors," ASME *Journal of Mechanical Design*, Vol. 101, pp. 640-644.

Childs, D. W., 1982, "Fractional-Frequency Rotor Motion Due to Nonsymmetric Clearance Effects," ASME *Journal of Engineering for Power*, Vol. 104, pp. 533-541.

Cunningham, W. J., 1958, *Introduction to Nonlinear Analysis*, McGraw-Hill Book Co., New York, NY.

Ehrich, F. F., 1966, "Subharmonic Vibration of Rotors in Bearing Clearance," ASME Paper 66-MD-1.

Ehrich, F. F., 1988, "High Order Subharmonic Response of High Speed Rotors in Bearing Clearance," ASME *Journal of Vibration, Acoustics, Stress, and Reliability in Design*, Vol. 110, pp. 9-16.

Ehrich, F. F., 1991, "Some Observations of Chaotic Vibration Phenomena in High-Speed Rotordynamics," ASME *Journal of Vibration, Acoustics, Stress, and Reliability in Design*, Vol. 113, pp. 50-57.

Gelin, A., Pugnet, J. M., and Hagopian, J. D., 1990, "Dynamic Behavior of Flexible Rotors with Active Magnetic Bearings on Safety Auxiliary Bearings," *Proceedings of 3rd International Conference on Rotordynamics*, Lyon, France, pp. 503-508.

Ishii, T., and Kirk, R. G., 1991, "Transient Response Technique Applied to Active Magnetic Bearing Machinery During Rotor Drop," *DE- Vol. 35, Rotating Machinery and Vehicle Dynamics, ASME*, pp.191-199.

Muszynska, A., 1984, "Partial Lateral Rotor to Stator Rubs, " IMechE Paper No. C281/84.

Yamamoto, T. T., 1954, "On Critical Speeds of a Shaft," *Memoirs of the Faculty of Engineering*, Nagoya University (Japan), Vol. 6, No. 2.

TABLE 1. FEM MODEL DATA

Station (in.)	O.D. (in.)	I.D. (in.)	WT. (lb)	Polar Mom. (lb.in.s^2)
5.400	2.800	2.000	0.000	0.000
5.450	2.800	2.000	5.000	5.000
6.500	2.800	2.000	0.000	0.000
6.505	7.300	6.950	0.100	0.100
7.100	7.300	6.950	0.000	0.000
8.670	7.300	7.120	30.400	425.000
10.900	8.400	8.220	0.000	0.000
13.120	9.300	9.120	0.000	0.000
15.310	10.100	9.920	20.300	538.000
17.280	10.700	10.550	9.150	302.000
18.580	11.200	11.050	0.000	0.000
19.880	11.550	11.400	0.000	0.000
21.120	11.950	11.800	0.000	0.000
22.380	12.150	12.000	41.900	1645.000
23.670	12.400	12.250	0.000	0.000
24.900	12.500	12.350	0.000	0.000
26.120	12.500	12.350	0.000	0.000
27.400	12.500	12.350	22.550	539.000
27.750	12.500	2.500	1.027	0.000
27.800	4.500	2.500	7.733	0.000
32.000	4.500	2.500	25.022	49.761
37.000	4.500	2.500	17.961	0.000
43.000	4.500	2.500	17.961	0.000
48.000	4.500	2.500	16.328	0.000
53.000	4.500	2.500	16.328	0.000
58.000	4.500	2.500	14.614	0.000
61.950	4.500	2.500	6.531	0.000
62.000	6.000	2.500	0.954	0.000
62.405	6.000	5.670	34.935	1216.500
64.600	6.000	5.670	0.000	0.000
67.000	6.000	5.670	117.000	3750.500
69.500	6.000	5.670	0.000	0.000
69.505	2.850	1.250	0.000	0.000
72.500	2.850	1.250	10.197	12.000
73.600	2.850	1.250	0.000	0.000

Modulus of elasticity: E=2.80e+7 psi
Shear Modulus of elasticity: G=1.08e+7 psi

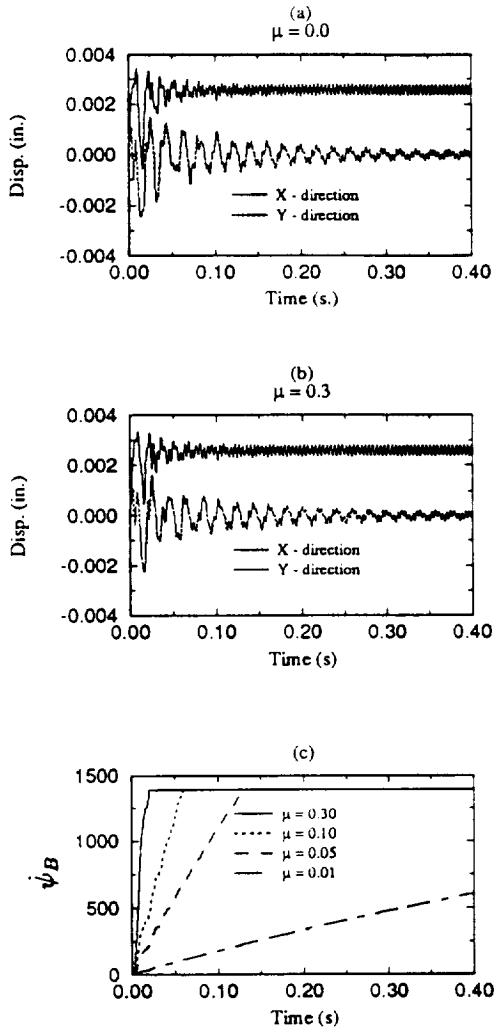

FIG. 3 EFFECTS OF BEARING FRICTION (C_B=157.0, K_B=0.313e+6, Ω=1400, δ=0.002, e=0.0002)

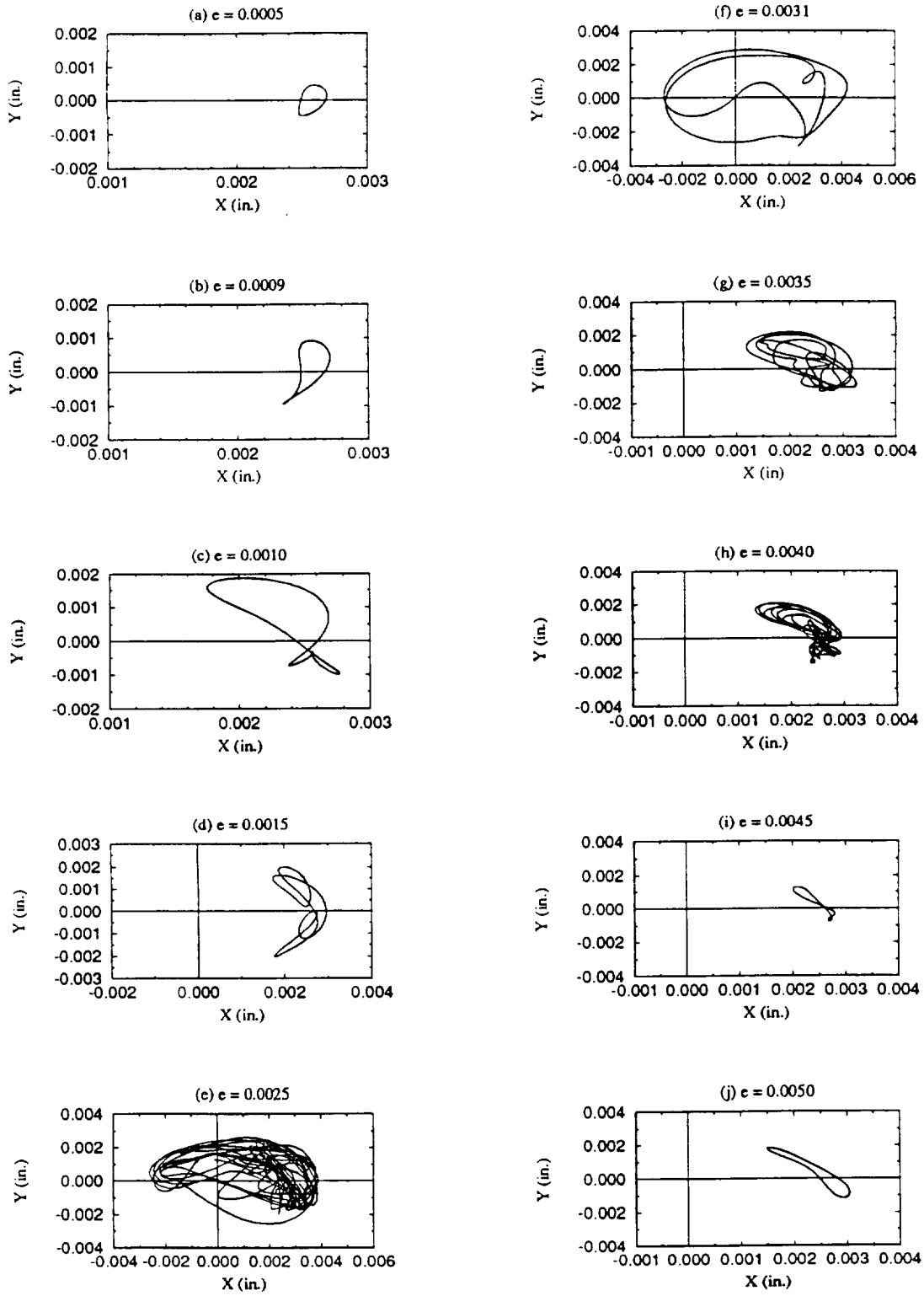

FIG. 4 IMBALANCE RESPONSES - ORBITS
(δ=0.002, K_B=0.313e+6, C_B=157.0)

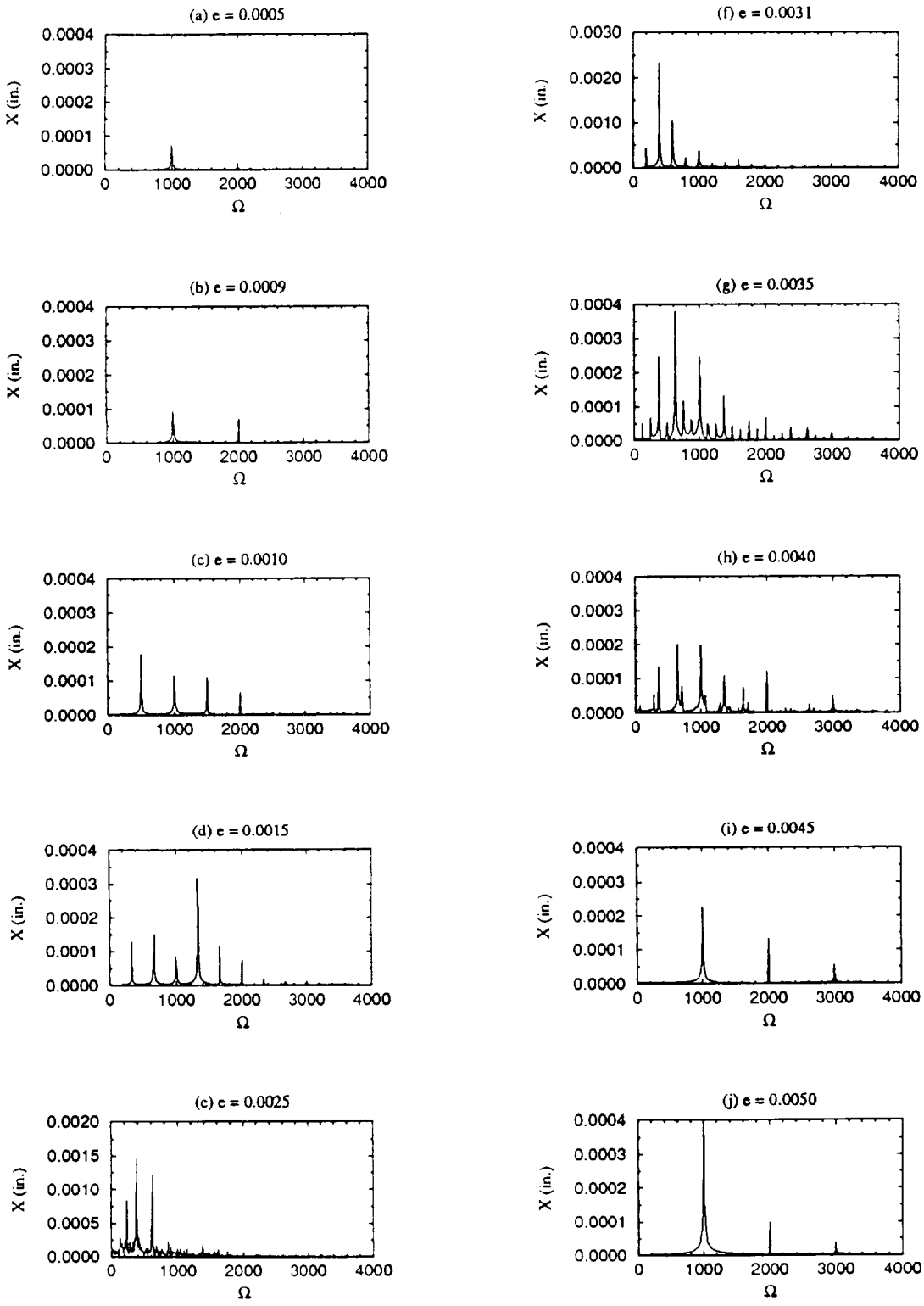

FIG. 5 IMBALANCE RESPONSES - SPECTRA
(δ=0.002, K_B=0.313e+6, C_B=157.0)

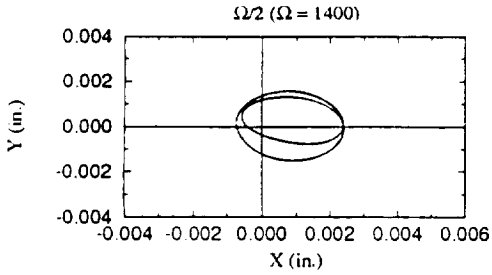

(a) δ=0.001, e=0.0007, C_B=157.0,

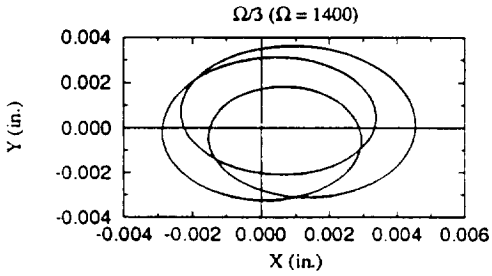

(b) δ=0.001, e=0.0029, C_B=157.0,

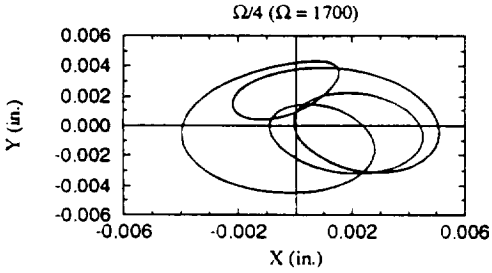

(c) δ=0.002, e=0.00105, C_B=145.0,

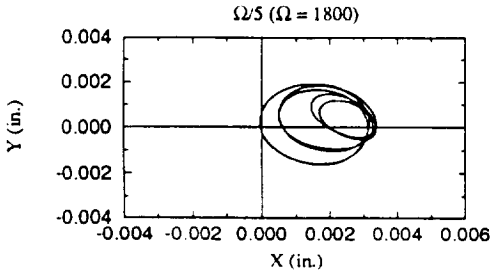

(d) δ=0.002, e=0.00067, C_B=157.0,

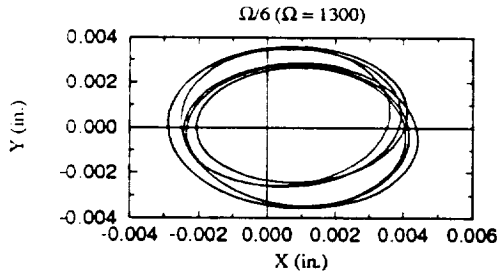

(e) δ=0.002, e=0.0025, C_B=157.0,

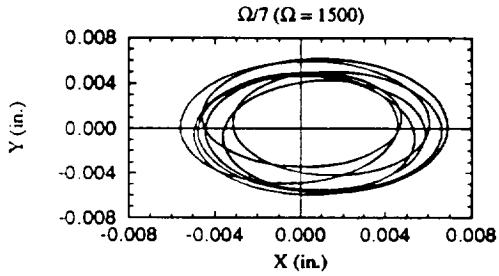

(f) δ=0.002, e=0.0032, C_B=157.0,

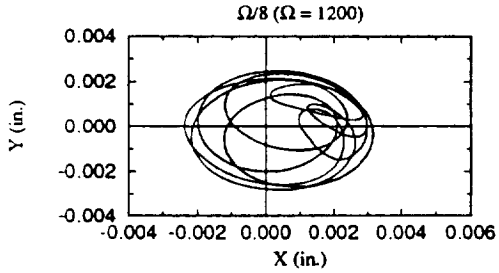

(g) δ=0.001, e=0.0030, C_B=157.0,

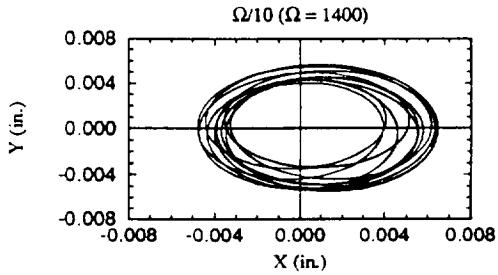

(h) δ=0.002, e=0.00395, C_B=157.0,

FIG. 7 SUBHARMONIC RESPONSES (ORBITS)
(K_B=0.313e+6)

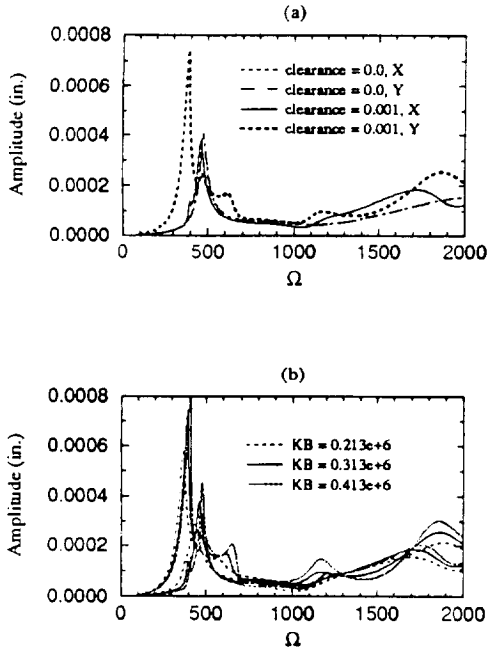

FIG. 8 INFLUENCE ON CRITICAL SPEEDS
(a) e=0.0001, C_B=157.0, K_B=0.313e+6
(b) e=0.0001, C_B=157.0, δ=0.001

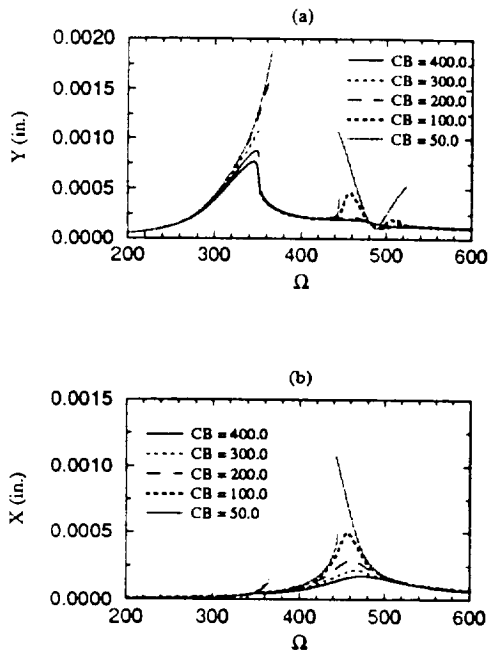

FIG. 10 EFFECTS OF BACK-UP BEARING DAMPING
(δ=0.002, e=0.0001, K_B=0.313e+6)

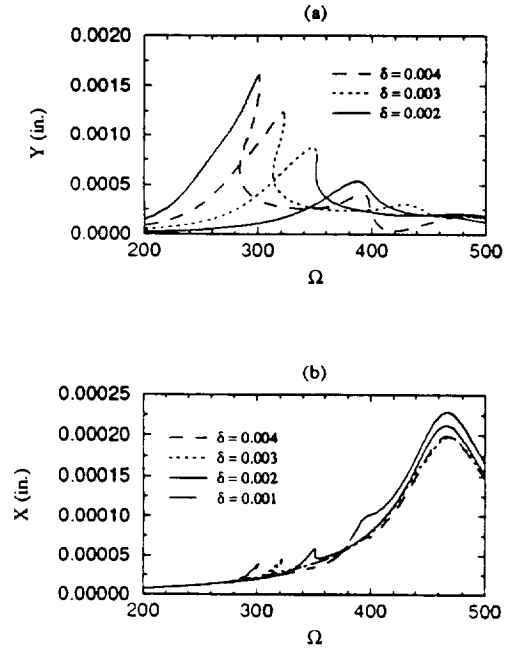

FIG. 9 CLEARANCE EFFECT ON JUMP PHENOMENA
(e=0.0001, K_B=0.313e+6, C_B=300.0)

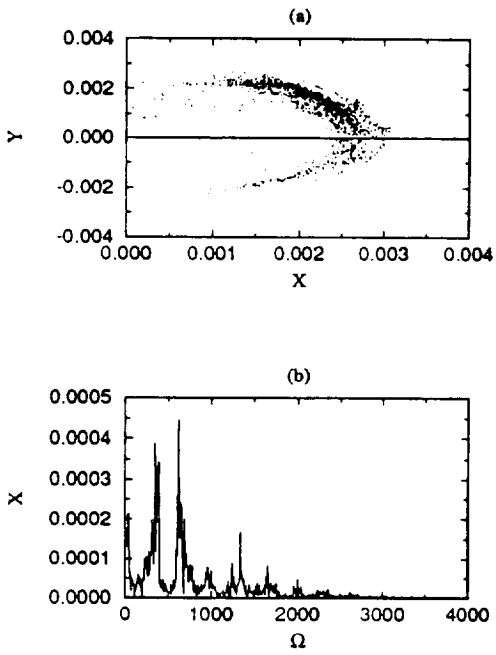

FIG. 6 CHAOTIC RESPONSES (e = 0.0023,
δ=0.002, K_B=0.313e+6, C_B=157.0)

OMIT

TSI Press Series

FIRST INDUSTRY/ACADEMY SYMPOSIUM ON RESEARCH FOR FUTURE SUPERSONIC AND HYPERSONIC VEHICLES

Applications, Design, Development, and Research

Held December 4-6, 1994 in Greensboro, North Carolina, U.S.A.

Volume 1

Editors:

Abdollah Homaifar
Department of Electrical Engineering
North Carolina A&T State University

John C. Kelly, Jr.
Department of Electrical Engineering
North Carolina A&T State Unversity

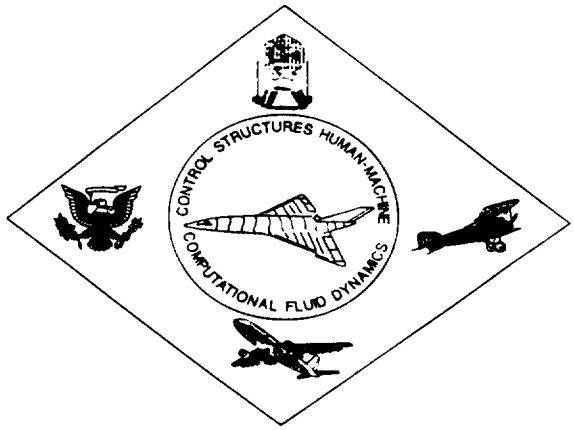

TSI Press Albuquerque, New Mexico USA 1994

Presented at: First Industry/University Symposium
on High Speed Transport Vehicles
Greensboro, North Carolina
December 4-6, 1994

DYNAMIC BEHAVIOR OF A MAGNETIC BEARING SUPPORTED JET ENGINE ROTOR WITH AUXILIARY BEARINGS

G.T. Flowers
H. Xie
S.C. Sinha

Department of Mechanical Engineering
Auburn University
Auburn, Alabama

ABSTRACT

This paper presents a study of the dynamic behavior of a rotor system supported by auxiliary bearings. The steady-state behavior of a simulation model based upon a production jet engine is explored over a wide range of operating conditions for varying rotor imbalance, support stiffness and damping. Interesting dynamical phenomena, such as chaos, subharmonic responses, and double-valued responses, are presented and discussed.

KEYWORDS: magnetic bearings, auxiliary bearings, nonlinear rotordynamics.

NOMENCLATURE

C_B = auxiliary bearing support damping, lb.s/in.
F_n = normal force, lb
$\mathbf{F}_X$ = external force vector acting on the rotor in X direction
$\mathbf{F}_Y$ = external force vector acting on the rotor in Y direction
$\mathbf{I}_a$ = rotor inertia matrix
K_B = auxiliary bearing support stiffness, lb/in.
K_C = contact stiffness, lb/in.
M_B = auxiliary bearing mass, lb.s^2/in.
M_k = mass of kth rotor element, lb.s^2/in.
N = total number of modes considered
N_{B1} = node number at auxiliary bearing #1
N_{B2} = node number at auxiliary bearing #2
$\mathbf{Q}_X$ = rotor modal coordinate vector in X direction
$\mathbf{Q}_Y$ = rotor modal coordinate vector in Y direction
R_B = radius of auxiliary bearing bore, in.
R_R = radius of rotor journal, in.
$\mathbf{X}_R$ = rotor physical coordinate vector in X direction
$\mathbf{Y}_R$ = rotor physical coordinate vector in Y direction
e = rotor imbalance eccentricity, in.
g = gravitational acceleration, in./s^2
t = time, s
Δ = deformation at the contact point, in.
$\mathbf{\Gamma} = \mathbf{\Psi}^T \mathbf{I}_a \mathbf{\Psi}$
$\mathbf{\Psi}$ = rotor free-free modal rotation matrix
Ω = rotor operating speed, rad/s
$\mathbf{\Phi}$ = rotor free-free modal displacement matrix
$\delta = R_B - R_R$, auxiliary bearing clearance, in.

ζ = modal damping coefficient

INTRODUCTION

Active magnetic bearings are one of the most innovative recent developments in the turbomachinery field. This technology provides the potential for significant improvements over other types of rotor support, including elimination of wear and bearing friction-related energy losses as well as a means of actively suppressing rotor vibration. A critical component of any magnetic bearing design is the auxiliary bearing, which protects the soft iron core of the magnetic bearing and provides rotor support in case of overload or failure of the primary (magnetic) bearing. Magnetic bearing systems appear to provide particularly great promise for use in aeronautical applications. In this regard, current effort is directed toward developing jet engines with rotors supported by magnetic bearings. For such applications, safety is an important concern. Toward this end, it is desirable to design the system to operate with auxiliary bearing support for an extended period of time.

A number of different bearing types have been suggested as auxiliary bearings. These include bushings, rolling element bearings, and various types of journal bearings. The most commonly considered are rolling element bearings. The major disadvantage associated with using rolling element bearings (or bushings) is the requirement of a clearance between the rotor and the inner race of the bearing, without which many of the advantages associated with using magnetic bearings would be reduced or eliminated. This clearance introduces a nonlinear dynamical feature which may significantly impact the behavior of the rotor.

There are quite a number of studies in the literature concerned with nonlinear rotordynamics. Yamamoto (1954) conducted a systematic study of rotor responses involving bearing clearance effects. Black (1968) studied the rotor/stator interaction with a clearance. Ehrich (1966, 1988 and 1991), Bently (1974), Muszynska (1984) and Childs (1979 and 1982) observed and studied subharmonic responses associated with clearance effects. While this work has served to greatly enhance the understanding of such systems, more detailed study is needed. Much of this earlier work was conducted from the perspective that the clearance is a result of manufacturing error or misfitting and is best eliminated. However, in a rotor system fitted with magnetic bearings and auxiliary bearings, the clearance becomes a design parameter rather than an irregularity. From this point of view, it is important to develop a better understanding of the expected dynamic responses. Such knowledge will provide guidelines for the selection of auxiliary bearing parameters.

There has been relatively little work available in the open literature that is specifically concerned with auxiliary bearings. Two papers that are directly related to research on auxiliary bearings are Gelin et al., (1990) and Ishii and Kirk (1991). Both of these papers are mainly concerned with transient responses. The current work is specifically concerned with developing a better understanding of the expected steady-state dynamical behavior for an auxiliary bearing supported rotor. Simulation results for a rotor based upon a production jet engine are presented and discussed.

The model used in the current study has two principal components - the rotor and the auxiliary bearings. The rotor is modelled using the free-free bending mode shapes and natural frequencies obtained through finite element analysis. The finite element code uses 34 stations and the first four modes (two rigid body and two flexible modes) are included in the simulation model. Figure 1 shows a schematic diagram of the finite element model. The rotor equations of motion can be expressed in terms of modal coordinates as:

$$\ddot{\mathbf{Q}}_X + 2\zeta\omega_n\dot{\mathbf{Q}}_X + \Omega\boldsymbol{\Gamma}\dot{\mathbf{Q}}_Y + \omega_n^2\mathbf{Q}_X + 2\Omega\zeta\omega_n\mathbf{Q}_Y = \boldsymbol{\Phi}^T\mathbf{F}_X, \tag{1.a}$$

$$\ddot{\mathbf{Q}}_Y + 2\zeta\omega_n\dot{\mathbf{Q}}_Y - \Omega\boldsymbol{\Gamma}\dot{\mathbf{Q}}_X + \omega_n^2\mathbf{Q}_Y - 2\Omega\zeta\omega_n\mathbf{Q}_X = \boldsymbol{\Phi}^T\mathbf{F}_Y. \tag{1.b}$$

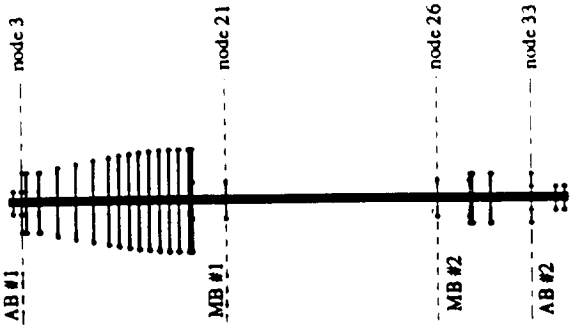

FIGURE 1 DIAGRAM OF THE FINITE ELEMENT MODEL

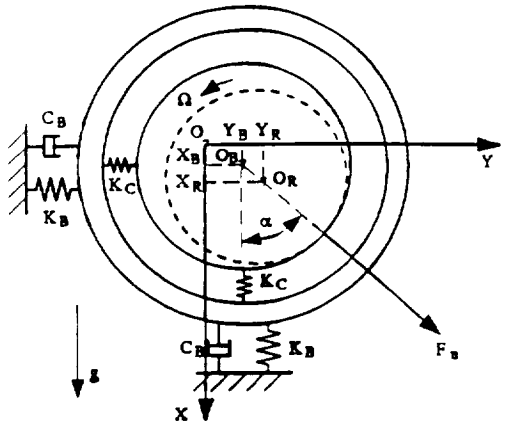

FIGURE 2 AUXILIARY BEARING MODEL

where

$$\mathbf{F}_X = \{F_{X1}, F_{X2}, \ldots, F_{Xm}\}^{-T},$$
$$\mathbf{F}_Y = \{F_{Y1}, F_{Y2}, \ldots, F_{Ym}\}^{-T},$$
$$\mathbf{Q}_X = \Phi^{-1}\mathbf{X}_R,$$
$$\mathbf{Q}_Y = \Phi^{-1}\mathbf{Y}_R,$$
$$\omega_n = \begin{pmatrix} \omega_{n_1} & 0 & \ldots & 0 \\ 0 & \omega_{n_2} & \ldots & 0 \\ \ldots & \ldots & \ldots & \ldots \\ 0 & 0 & \ldots & \omega_{n_N} \end{pmatrix}$$

with

$$\mathbf{X}_R = \{X_{R1}, X_{R2}, \ldots, X_{Rm}\}^{-T},$$
$$\mathbf{Y}_R = \{Y_{R1}, Y_{R2}, \ldots, Y_{Rm}\}^{-T}.$$

(m = total number of nodes)

The physical displacements of the rotor at the two auxiliary bearing locations can be obtained using the following coordinate transformation:

$$X_{Rk} = \sum_{i=1}^{N} \Phi_{ki} Q_{Xi},$$
$$Y_{Rk} = \sum_{i=1}^{N} \Phi_{ki} Q_{Yi}, \qquad (k = N_{B1}, N_{B2})$$

The model for the auxiliary bearings is shown in Figure 2. The governing equations of motion are:

$$M_{Bk}\ddot{X}_{Bk} + C_{Bk}\dot{X}_{Bk} + K_{Bk}X_{Bk} = F_{nk}\cos\alpha_k + M_{Bk}g, \qquad (2.a)$$
$$M_{Bk}\ddot{Y}_{Bk} + C_{Bk}\dot{Y}_{Bk} + K_{Bk}Y_{Bk} = F_{nk}\sin\alpha_k, \qquad (2.b)$$

where

$$\alpha_k = tan^{-1} \frac{Y_{Rk} - Y_{Bk}}{X_{Rk} - X_{Bk}}.$$
$$(k = N_{B1}, N_{B2})$$

$$F_{Xk} = - F_{nk} \cos \alpha_k + M_k \, g + M_k \, e \, \Omega^2 \cos(\Omega t),$$
$$F_{Yk} = - F_{nk} \sin \alpha_k + M_k \, e \, \Omega^2 \sin(\Omega t).$$

The rotor/bearing interaction is represented with the normal force F_{nk}

$$F_{nk} = \begin{cases} K_C \delta_k, & \Delta_k > 0, \\ 0, & \Delta_k \leq 0, \end{cases} \tag{3}$$

where

$$\Delta_k = (X_{Rk} - X_{Bk}) \cos \alpha_k + (Y_{Rk} - Y_{Bk}) \sin \alpha_k - \delta_k.$$

DISCUSSION OF RESULTS

The model described in the previous section was used to study the steady-state dynamic behavior of such a system using direct numerical integration of the equations and a harmonic balance code. Studies were performed for varied values of imbalance, support stiffness, and support damping, respectively. For the purposes of the current work, the two auxiliary bearings are located at nodes 3 and 33, respectively. It is assumed that they are identical in terms of stiffness, damping and friction characteristics. The nominal system parameters used for the simulation study are M_{B1}=0.0023, M_{B2}=0.0024, K_C=2.855e+6, and ζ=0.03. All the results that are presented correspond to node 3, the location of bearing 1.

The dynamical behavior of a rotor supported by bearings with clearance coupled with the nonsymmetry resulting from gravitational effects can be quite complex. The harmonic balance method is first used to investigate the synchronous behavior for small imbalance values. (Please note that the complex frequency contents associated with medium and large imbalance values makes it a formidable task to apply the harmonic balance method for other cases.) Figure 3 is a typical plot of the steady state response amplitudes as functions of the rotor speed with and without bearing clearance. The nonsymmetric effects resulting from gravity loading is similar to what occurs for a rotor supported by nonsymmetric bearing stiffnesses with regard to influence on critical speeds. The first critical speed splits into two distinct values. For the X direction, the gravity force tends to keep the rotor in contact with the bearing at low operating speed. The apparent stiffness in this direction is approximately the same as K_B and the resulting critical speed about the same as the critical speed for the linear case (δ=0). For the Y direction, the clearance results in a lower apparent stiffness and a lower critical speed. Several higher order pseudo-critical speeds are also created in the operating speed range (about 1500 rad./sec). It should be noted that the response in the X direction also departs from the linear case at high operating speed. This is because the imbalance force becomes dominant at high rotor speed which in turn makes the gravity force less significant and the clearance effect more important.

Figure 4(a) shows some typical results for varying imbalance. Some of the more dynamically interesting results occur for cases of relatively large imbalance. It is observed that imbalance may influence the frequency content of the rotor responses quite dramatically at certain operating speeds. There exists as many as eight ranges of imbalance values that result in eight different types of rotor responses. In fact, subharmonic responses from $\Omega/2$ through $\Omega/10$ are observed. Those subharmonics are not directly related to the system's natural frequencies as were the cases with other researchers' findings (such as Ehrich, 1988). Moreover, several types of subharmonic responses may occur for identical parametric configurations, but different imbalance values.

Figures 4(b) and 4(c) show typical results using K_B or C_B as the variable parameter. Clear routes to chaos are observed. As K_B increases beyond certain value, a period-doubling bifurcation always

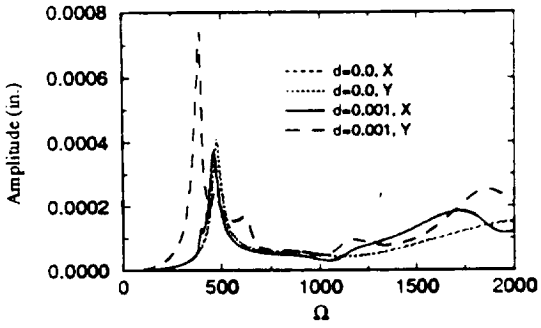

FIGURE 3 INFLUENCE OF CLEARANCE ON CRITICAL SPEEDS
(e=0.0001, C_B=150.0, K_B=0.313x10^6)

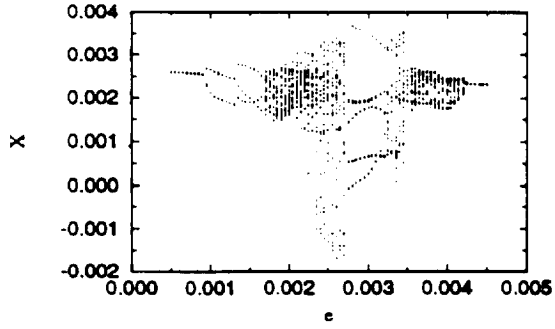

FIGURE 4(a) BIFURCATION DIAGRAM WITH IMBALANCE AS THE VARIABLE PARAMETER
(Ω=1000, δ=0.002, C_B=150, K_B=0.313x10^6)

takes place. As C_B decreases below certain value, the responses always become chaotic. However, the bifurcation type is not well defined as for varied K_B. It should be pointed out that even though a lower K_B may leads to a better system response, it may also fail to protect the magnetic bearings due to the fact that it could result in a larger rotor orbit-center offset. In addition, higher bearing damping does not necessarily result in synchronous responses. It is observed that, with small imbalance ($e \leq 0.0005$), the responses are always synchronous for all speeds in the speed range considered ($\leq$ 1800) if C_B is large enough (C_B=250.0) and the clearance is small enough ($\delta \leq 0.001$). As with the other cases, higher bearing damping or lower bearing stiffness or lower imbalance tends to increase the probability of synchronous responses.

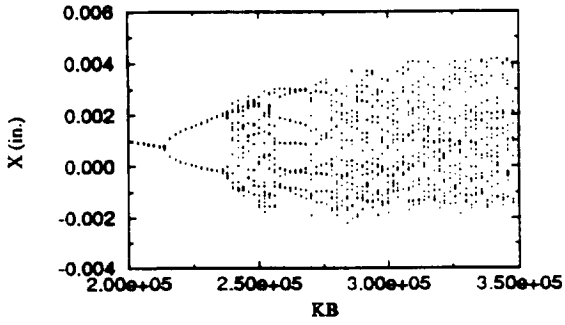

FIGURE 4(b) BIFURCATION DIAGRAM WITH BEARING STIFFNESS AS THE VARIABLE PARAMETER
(Ω=1500, δ=0.002, C_B=150, e=0.0008)

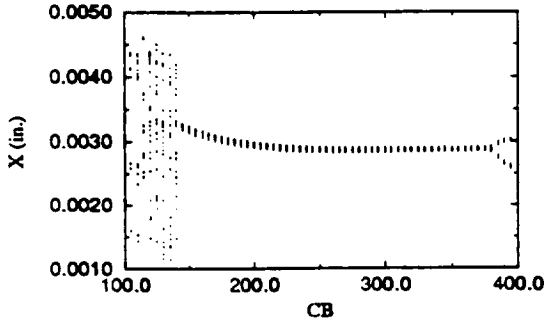

FIGURE 4(c) BIFURCATION DIAGRAM WITH BEARING DAMPING AS THE VARIABLE PARAMETER
(Ω=1500, δ=0.002, e=0.0015, K_B=0.313x10^6)

CONCLUSIONS

As a summary of the results discussed above, the following conclusions can be drawn:

1. Imbalance may serve to dramatically alter the frequency contents of the rotor responses at certain operating speeds. This is particularly evident for cases of large clearance, high bearing stiffness and low bearing damping.
2. For sufficiently high imbalance:
   i. There is a threshold level of damping below which complex dynamical behavior can be expected.
   ii. There is a threshold level of stiffness above which complex dynamical behavior can be expected.
3. Clear routes to chaos are observed. As bearing stiffness increases beyond a certain value, a period-doubling bifurcation takes place which leads to chaos. As bearing damping decreases below a certain value, chaos also tends to occur but the bifurcation type is not so clearly defined.

ACKNOWLEDGEMENT

The authors would like to express their gratitude to S. A. Klusman of the Allison Engine Company for many helpful discussions and practical advice.
This work was supported by NASA under Grant No. NAG3-1507. The Government has certain rights in this material.

REFERENCES

Bently, D. E., 1974, "Forced Subrotative Speed Dynamic Action of Rotating Machinery," ASME Paper No. 74-PET-16.
Black, H. F., 1968, "Interaction of a Whirling Rotor With a Vibrating Stator Across a Clearance Annulus," *Journal of Engineering Science*, Vol. 10, No. 1, pp. 1-12.
Childs, D. W., 1979, "Rub-Induced Parametric Excitation in Rotors," ASME *Journal of Mechanical Design*, Vol. 101, pp. 640-644.
Childs, D. W., 1982, "Fractional-Frequency Rotor Motion Due to Nonsymmetric Clearance Effects," ASME *Journal of Engineering for Power*, Vol. 104, pp. 533-541.
Ehrich, F. F., 1966, "Subharmonic Vibration of Rotors in Bearing Clearance," ASME Paper 66-MD-1.
Ehrich, F. F., 1988, "High Order Subharmonic Response of High Speed Rotors in Bearing Clearance," ASME *Journal of Vibration, Acoustics, Stress, and Reliability in Design*, Vol. 110, pp. 9-16.
Ehrich, F. F., 1991, "Some Observations of Chaotic Vibration Phenomena in High-Speed Rotordynamics," ASME *Journal of Vibration, Acoustics, Stress, and Reliability in Design*, Vol. 113, pp. 50-57.
Gelin, A., Pugnet, J. M., and Hagopian, J. D., 1990, "Dynamic Behavior of Flexible Rotors with Active Magnetic Bearings on Safety Auxiliary Bearings," *Proceedings of 3rd International Conference on Rotordynamics*, Lyon, France, pp. 503-508.
Ishii, T., and Kirk, R. G., 1991, "Transient Response Technique Applied to Active Magnetic Bearing Machinery During Rotor Drop," *DE- Vol. 35, Rotating Machinery and Vehicle Dynamics, ASME*, pp.191-199.
Muszynska, A., 1984, "Partial Lateral Rotor to Stator Rubs," IMechE Paper No. C281/84.
Yamamoto, T. T., 1954, "On Critical Speeds of a Shaft," *Memoirs of the Faculty of Engineering*, Nagoya University (Japan), Vol. 6, No. 2.

To be presented at: 15th Biennial ASME Vibrations Conference
Boston, Massachusetts
September 17-21, 1995

DYNAMIC MODELLING AND RESPONSE CHARACTERISTICS OF A MAGNETIC BEARING ROTOR SYSTEM WITH AUXILIARY BEARINGS

April M. Free and George T. Flowers

Department of Mechanical Engineering
Auburn University
Auburn, AL 36849

Victor S. Trent

Department of Electrical Engineering
Auburn University
Auburn, AL 36849

ABSTRACT

Auxiliary bearings are a critical feature of any magnetic bearing system. They protect the soft iron core of the magnetic bearing during an overload or failure. An auxiliary bearing typically consists of a rolling element bearing or bushing with a clearance gap between the rotor and the inner race of the support. The dynamics of such systems can be quite complex. It is desired to develop a rotordynamic model which describes the dynamic behavior of a flexible rotor system with magnetic bearings including auxiliary bearings. The model is based upon an experimental test facility. Some simulation studies are presented to illustrate the behavior of the model. In particular, the effects of introducing sideloading from the magnetic bearing when one coil fails is studied. These results are presented and discussed.

NOMENCLATURE

C = damping, N-s/m
C_L = clearance of auxiliary bearing, m
D = nominal gap thickness, m
$\mathbf{F}_X$ = external force vector acting on the rotor in X direction, N
$\mathbf{F}_Y$ = external force vector acting on the rotor in Y direction, N
G = gravitational acceleration, m/s^2
I = rotor inertia matrix
i = current, amp
K = stiffness, N/m
k = gain value
L = equivalent circuit length
M = mass, kg
m = total number of nodes
N = total number of modes considered
N_{B1} = node number at rotor left end
N_{B2} = node number at AMB
N_{B3} = node number at auxiliary bearing
N_{imb} = node number at imbalance location
N_T = number of turns of wire per coil
$\mathbf{Q}_X$ = rotor modal coordinate vector in X direction
$\mathbf{Q}_Y$ = rotor modal coordinate vector in Y direction
R_R = radius of rotor journal, m.
R_S = radius of auxiliary bearing bore, m.
t = time, s
t_f = fail time, s
v = voltage, volt
v_r = relative velocity at auxiliary bearing rotor/stator contact point
$\mathbf{X}_R$ = rotor physical coordinate vector in X direction
$\mathbf{X}_S$ = stator physical coordinate vector in X direction
$\mathbf{Y}_R$ = rotor physical coordinate vector in Y direction
$\mathbf{Y}_S$ = stator physical coordinate vector in Y direction
α = acceleration, rad/sec^2
δ = dynamic clearance

$\Gamma = \Psi^T I \Psi$
Φ = rotor free-free modal displacement matrix
Ψ = rotor free-free modal rotation matrix
ψ = imbalance vector
μ_o = permeability of free space
μ_r = permeability of silicon steel
Ω = rotor operating speed, rad/s
τ = time constant
θ = angular position of the shaft
ζ = modal damping coefficient

Subscripts

a = first
B = auxiliary bearing
b = second
C = contact
g = gain constant
h = horizontal
l = left bearing
r = rate constant
v = vertical
x = x – direction
y = y – direction
bi = bias
1 = top magnet
2 = right magnet
3 = bottom magnet
4 = left magnet

Superscripts

a = current amplifier
c = controller
l = lead
p = sensor amplifier

INTRODUCTION

In recent years, the use of active magnetic bearings (AMB) for turbomachinery support has been an area of interest in both academia and in industry. Magnetic bearings provide the potential for significant improvements over other types of rotor supports, including elimination of wear, bearing friction-related energy losses and a means of actively suppressing rotor vibration. A critical feature of any magnetic bearing supported rotor system is auxiliary bearings to protect the soft iron core from rotor contact (and subsequent damage) during an overload or failure of the AMB. The present work is concerned with developing a suitable model and investigating the dynamic behavior of such a system.

EXPERIMENTAL TEST FACILITY

The model and control system development presented in this study is for an experimental test facility. The apparatus consists of a radial magnetic bearing that is supporting the right end of a rotor. The left end of the rotor is supported by a ball bearing suspended in a frame by four springs. A photograph and the corresponding schematic diagram are shown in Figure 1.

The apparatus has two basic components: the rotor shaft and the magnetic bearing. The shaft is made of steel and is 0.0098 meters in diameter and 0.4572 meters in length. A steel disk of diameter 7.62 cm, thickness 2.54 cm, and mass 0.810 kg is placed at the midpoint of the bearing span. Threaded holes on the disk allow for imbalance to be added to the system. The rotor is driven by a variable speed motor with a controller. Shaft vibration is measured using eddy current proximity displacement sensors fixed to measure displacement in both the vertical and horizontal directions.

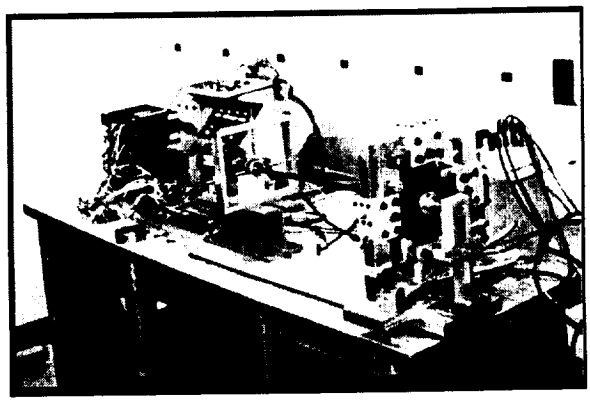

Figure 1.a Experimental Test Facility

The magnetic bearing is based upon a design described in Humphris, et al (1988). The basic parameters for the bearing are shown in Table 1. The bearing consists of four electromagnets equally spaced around a soft–iron core. A photograph and schematic diagram of the bearing are shown in Figure 2.

SIMULATION MODEL

A simulation model was developed for the rotor system described above. The model has three principal components – the rotor, magnetic bearing, and electronics. The governing equations for each are shown below.

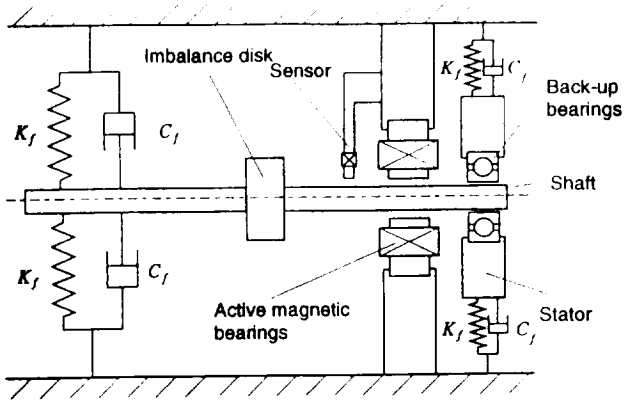

Figure 1.b Schematic Diagram of Experimental Test Facility

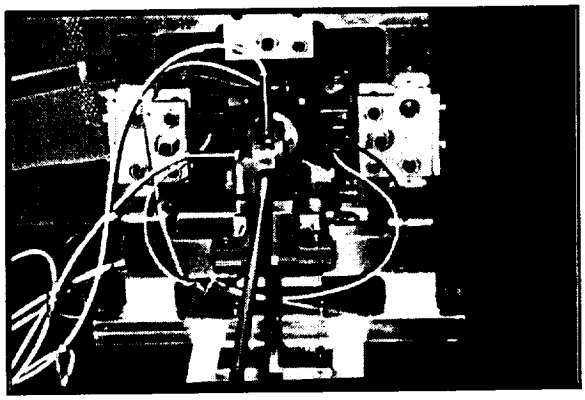

Figure 2.a Magnetic Bearing Assembly

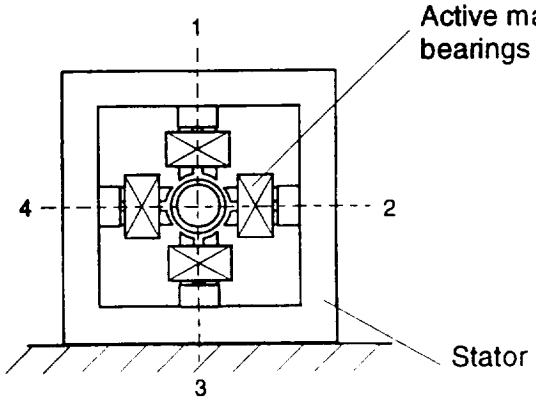

Figure 2.b Schematic Diagram of Magnetic Bearing

The rotor is modelled using the free-free bending mode shapes and natural frequencies obtained through finite element analysis. The finite element code uses 11 stations and the first four modes (two rigid body and two flexible modes) are included in the simulation model. The rotor equations of motion can be expressed in terms of modal coordinates as

$$\ddot{\mathbf{Q}}_x + \Omega\Gamma\dot{\mathbf{Q}}_y + \omega_n^2\mathbf{Q}_x + \Phi^T\mathbf{F}_x = 0, \quad (1.a)$$

$$\ddot{\mathbf{Q}}_y - \Omega\Gamma\dot{\mathbf{Q}}_x + \omega_n^2\mathbf{Q}_y + \Phi^T\mathbf{F}_y = 0, \quad (1.b)$$

The auxiliary bearing consists of a ball bearing with a clearance between the rotor and the stator. The governing equations are

$$M_B\ddot{X}_B + C_{Bx}\dot{X}_B + K_{Bx}X_B = \mathbf{F}_{x,aux}, \quad (1.c)$$

$$M_B\ddot{Y}_B + C_{By}\dot{Y}_B + K_{By}Y_B = \mathbf{F}_{y,aux}, \quad (1.d)$$

where

$$\mathbf{F}_{x,lin}(N_{b1}) = \Phi_{N_{b1}}(K_{lx}\mathbf{Q}_x + C_{lx}\dot{\mathbf{Q}}_x)$$

$$\mathbf{F}_{y,lin}(N_{b1}) = \Phi_{N_{b1}}(K_{ly}\mathbf{Q}_y + C_{ly}\dot{\mathbf{Q}}_y)$$

$$\mathbf{F}_{x,imb}(N_{imb}) = \Omega^2\psi_6 cos\theta + \alpha\psi_6 sin\theta,$$

$$\mathbf{F}_{y,imb}(N_{imb}) = \Omega^2\psi_6 sin\theta - \alpha\psi_6 cos\theta,$$

$$\mathbf{F}_{x,aux}(N_{b3}) = \Phi_{N_{b3}}(\mathbf{F}_N cos\beta - \mathbf{F}_R sin\beta)$$

$$\mathbf{F}_{y,aux}(N_{b3}) = \Phi_{N_{b3}}(\mathbf{F}_N sin\beta + \mathbf{F}_R cos\beta)$$

$$\mathbf{F}_{grav} = \Phi^T MG$$

$$\mathbf{F}_N = \phi K_c(\delta - \mathbf{D}).$$

If $v_r = 0$, then $\mathbf{F}_R$ = required static friction force to satisfy this condition. If $v_r \neq 0$ or if required static friction force $> \mu_s\mathbf{F}_N$, then $\mathbf{F}_R = \mu_k\mathbf{F}_N$.

$$\mathbf{F_x} = \mathbf{F}_{x,lin} + \mathbf{F}_{x,imb} + \mathbf{F}_{x,aux} - \mathbf{F}_{x,amb}$$

$$\mathbf{F_y} = \mathbf{F}_{y,lin} + \mathbf{F}_{y,imb} + \mathbf{F}_{y,aux} - \mathbf{F}_{y,amb} + \mathbf{F}_{grav}$$

where

$$\sin(\beta) = \frac{\mathbf{Y}_R - \mathbf{Y}_S}{\sqrt{(\mathbf{X}_R - \mathbf{X}_S)^2 + (\mathbf{Y}_R - \mathbf{Y}_S)^2}},$$

$$\cos(\beta) = \frac{\mathbf{X}_R - \mathbf{X}_S}{\sqrt{(\mathbf{X}_R - \mathbf{X}_S)^2 + (\mathbf{Y}_R - \mathbf{Y}_S)^2}},$$

$$\delta = \sqrt{(\Phi\mathbf{Q}_x - X_b)^2 + (\Phi\mathbf{Q}_y - Y_b)^2},$$

$$\phi = 1 \; if \; \delta > \Delta$$

$$0 \; otherwise$$

$$\mathbf{Q}_x = \Phi^T \mathbf{X}_r,$$

$$\mathbf{Q}_y = \Phi^T \mathbf{Y}_r,$$

with

$$\mathbf{X}_r = \{X_{r1}, X_{r2}, \ldots, X_{rm}\}^T,$$

$$\mathbf{Y}_r = \{Y_{r1}, Y_{r2}, \ldots, Y_{rm}\}^T.$$

The physical displacements of the rotor at the bearing and imbalance locations can be obtained using the following coordinate transformation:

$$X_{rk} = \sum_{i=1}^{N} \Phi_{ki} Q_{xi},$$

$$Y_{rk} = \sum_{i=1}^{N} \Phi_{ki} Q_{yi},$$

$$(k = N_{b1}, N_{b2}, N_{b3}, N_{imb})$$

The position of the shaft at the magnetic bearing location is measured using horizontal and vertical proximity sensors. They are modelled as linear first order systems.

$$\frac{dv_v^p}{dt} = \frac{k^p y - v_v^p}{\tau^p} \qquad (2.a)$$

$$\frac{dv_h^p}{dt} = \frac{k^p x - v_h^p}{\tau^p} \qquad (2.b)$$

The active control system is based upon a proportional–derivative (PD) control law and implemented using analog circuitry. The controller is modelled as

$$\frac{dv_v^c}{dt} = k_g v_v^p \tau^c + (k_g + k_r)\frac{v_v^p}{dt} - \tau^c v_v^c \; (3.a)$$

$$\frac{dv_h^c}{dt} = k_g v_h^p \tau^c + (k_g + k_r)\frac{v_h^p}{dt} - \tau^c v_h^c \; (3.b)$$

The control circuitry also includes a lead network. The governing equations are

$$\frac{dv_v^l}{dt} = \frac{1}{\tau_a^l} v_v^c + \frac{dv_v^c}{dt} - \frac{1}{\tau_b^l} v_v^l \qquad (4.a)$$

$$\frac{dv_h^l}{dt} = \frac{1}{\tau_a^l} v_h^c + \frac{dv_h^c}{dt} - \frac{1}{\tau_b^l} v_h^l \qquad (4.b)$$

Four current amplifiers (one for each coil) supply current to the magnetic bearing. They are modelled as

$$\frac{di_1^a}{dt} = -\frac{1}{\tau^a} i_1^a + \frac{1}{\tau^a} k_1^a v_v^l \qquad (5.a)$$

$$\frac{di_2^a}{dt} = -\frac{1}{\tau^a} i_2^a + \frac{1}{\tau^a} k_2^a v_v^l \qquad (5.b)$$

$$\frac{di_3^a}{dt} = -\frac{1}{\tau^a} i_3^a + \frac{1}{\tau^a} k_3^a v_h^l \qquad (5.c)$$

$$\frac{di_4^a}{dt} = -\frac{1}{\tau^a} i_4^a + \frac{1}{\tau^a} k_4^a v_h^l \qquad (5.d)$$

The forces supplied by the magnetic bearing to the rotor are assumed to be decoupled in the horizontal and vertical directions. The effects of flux saturation are included in the model based upon the approach described by Lewis (1993). The equations for these forces are

$$\mathbf{F}_{x,amb} = \mu_o A N_T^2 \left(\frac{i_2^2}{(2(D - x_{N_{B2}}) + \frac{L}{\mu_r})^2} - \frac{i_4^2}{(2(D + x_{N_{B2}}) + \frac{L}{\mu_r})^2} \right) \quad (6.a)$$

$$\mathbf{F}_{y,amb} = \mu_o A N_T^2 \left(\frac{i_1^2}{(2(D - y_{N_{B2}}) + \frac{L}{\mu_r})^2} - \frac{i_3^2}{(2(D + y_{N_{B2}}) + \frac{L}{\mu_r})^2} \right) \quad (6.b)$$

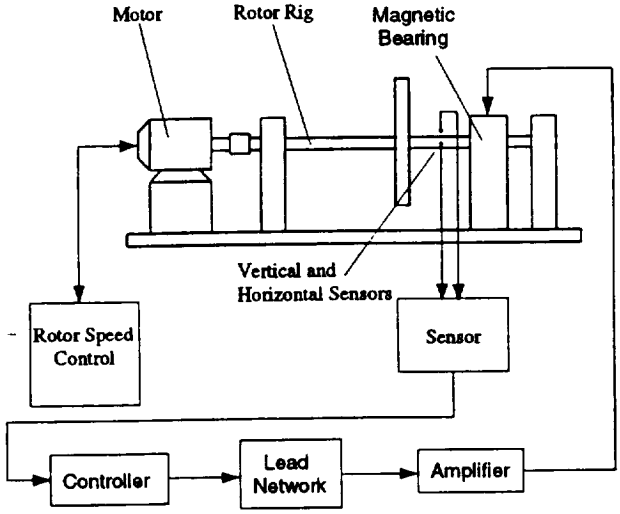

Figure 3 Block Diagram of Simulation Model

DISCUSSION

Using the rotordynamic model described in the preceding paragraphs, a study of the combined dynamics of a magnetic bearing supported rotor with auxiliary bearings was performed. The parameters used in this work were identified from experimental evaluation of the test rig and are shown in Table 1. All of the

Parameter	Value	Units
K_{lx}, K_{ly}	17,510	N/m
C_{lx}, C_{ly}	2.0	N-s/m
K_C	87,557	N/m
C_C	0	N-s/m
K_B	17,510	N/m
C_{Bx}, C_{By}	2.0	N-s/m
M_B	0.033	kg
ψ_6	3.0×10^{-6}	kg-m
k^p	7.8×10^{3}	-
k_g	13	-
k_r	23	-
k^a	0.45	amp/v
τ^p	1.59×10^{-5}	-
τ_a^l	1.8×10^{-3}	-
τ_b^l	1.59×10^{-4}	-
τ^a	5.31×10^{-5}	-
A	3.42×10^{-4}	m^2
N_T	164	-
D	0.9×10^{-3}	m
μ_o	1.26×10^{-6}	-
v_1^b	4.2	volt
v_2^{bi}	1.9	volt
v_3^{bi}	1.0	volt
v_4^{bi}	1.9	volt

Table 1 Simulation Model Parameters

responses illustrated in the figures are for this base parametric configuration, unless otherwise indicated. Figure 3 shows the variation of system natural frequencies with rotor speed for the base parametric configuration (without auxiliary bearing contact). The rotor speed of 200 rad/sec was selected as a reasonable value near a critical speed in order to illustrate a worst case behavior of the system.

Figure 4 shows the rotor response under normal operating conditions. The horizontal and vertical responses are of the same amplitude and frequency at steady state. The response consists of a transient region of about 0.5 seconds in length followed by steady synchronous oscillations. The initial conditions are set so that the rotor contacts the auxiliary bearing during the transient phase of the oscillations. The rotor vibrates downward, contacts the auxiliary bearing, bounces several times, and then settles into a steady synchronous whirl of about

0.05 mm in amplitude.

Of particular interest in this study is the use of the remaining coils of the AMB (when one fails) to provide a sideloading force to reduce rotor vibration. The test configuration consists of allowing coil 2 to fail and investigating the effects of sideloading on the system. Coils 1 and 3 are kept in the same electronic configuration as if no failure had occurred. However, the voltage in coil 4 is set to a value that will pull the shaft horizontally over to the auxiliary bearing. Two basic scenarios for rotor control during failure are considered. Figures 5.a – 5.c illustrate the rotor behavior under the conditions for the first scenario, when the rotor speed is maintained at a constant value. For each case, the AMB fails at t_f= 0.5 seconds. There is some perturbation of the vertical motion of the rotor when the horizontal coil fails due to coupling of the horizontal and vertical motion (primarily) through the gyroscopic terms. However, the steady state vertical responses are not significantly affected. Figures 6.a – 6.c show the rotor behavior for the same failure conditions (with sideloading) as above for the second scenario, when the rotor is decelerated at a constant rate upon AMB failure. Again the response amplitudes tend to be lowest for smaller clearance values. It is observed that the responses may be quite high as the rotor contacts the auxiliary bearing, even with sideloading from the remaining coil. However, sideloading is shown to be quite effective in encouraging rotor contact that will dissipate the vibrational energy. The response amplitudes tend to decrease as the auxiliary bearing clearance is decreased. However from a practical perspective, there are definite design tradeoffs that must be considered. If the clearance is too small, the rotor may strike the auxiliary bearing during normal operation of the magnetic bearing if the rotor is perturbed. This tends to unnecessarily shorten the life of the auxiliary bearing. If the clearance is too large, the rotor vibration (upon AMB failure) will be excessively high and may damage the rotor or the magnetic bearing structure.

The effect the sideloading voltage on the system dynamics is particularly interesting. The magnetic bearing forces are nonlinear functions of the dynamic clearance and the current. If one coil fails and the remaining coils are used to provide sideloading, the natural approach might seem to issue a constant command voltage, with the objective of having a constant sideloading force at steady state. However, the inherently unstable behavior of the magnetic bearing without active control coupled with the vibrational

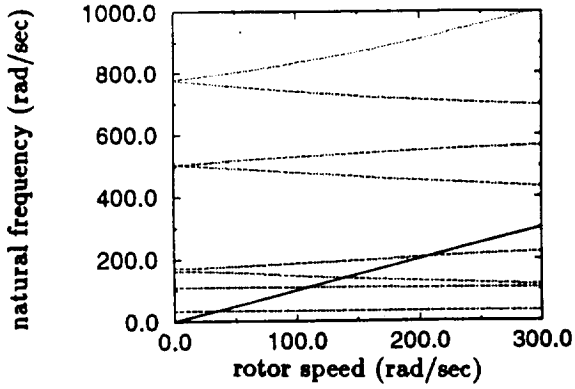

Figure 3 Rotor Natural Frequencies as a Function of Rotor Speed (for the parameters of Table 1)

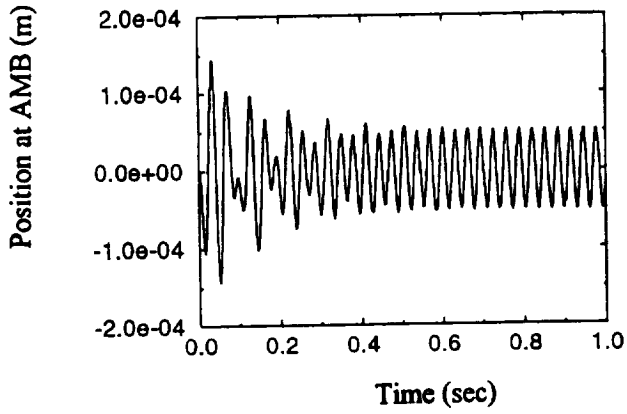

Figure 4 Rotor Response Without AMB Failure $\Omega = 200\text{rad/sec}, C_L = \frac{D}{2}$

effects between the auxiliary bearing and the rotor produces a severely unstable response. A remedy is to command a voltage that is proportional to the horizontal shaft displacement. That is, $v^a = v_o^a(D + x_{N_{B2}})$, where v_o^a is a constant. With an ideal amplifier, any value of v_o^a can be used with such a system. However due to the delay in the dynamics from the time constant of the power amplifier, unstable behavior may also result if v_o^a is too large. Figure 7 shows the maximum v_o^a that can be commanded with stable behavior as a function of power amplifier time constant. These results were developed by fitting a smooth curve through data points obtained by observing the behavior of the simulation model for various sideloading voltages and

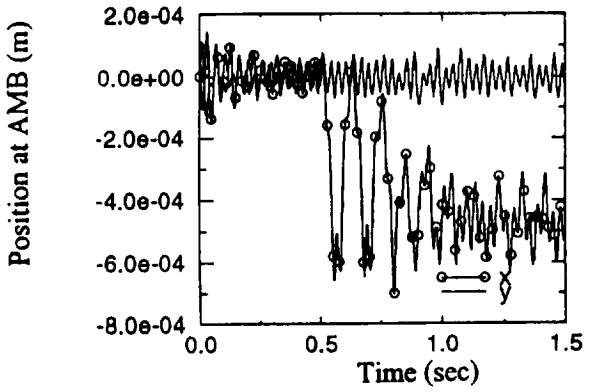

Figure 5.a Rotor Response With AMB Failure
$\Omega = 200\text{rad/sec}, C_L = \frac{2D}{3}$
$t_f = 0.5, \alpha = 0$

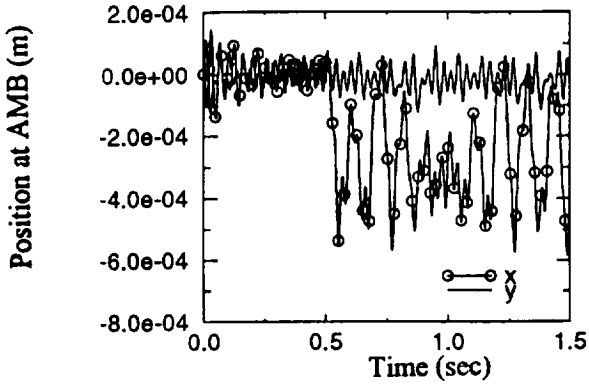

Figure 5.b Rotor Response With AMB Failure
$\Omega = 200\text{rad/sec}, C_L = \frac{D}{2}$
$t_f = 0.5, \alpha = 0$

amplifier time constants. It must be concluded that power amplifier dynamics are a critical factor in the selection of appropriate levels of bearing sideloading.

CONCLUSION

A simulation model has been developed for a magnetic bearing supported flexible rotor system with auxiliary bearings including frictional effects. The model has been described in detail with experimentally obtained model parameters. The response characteristics for a variety of system configurations were presented and discussed, including the effects of sideloading. Some guidelines were given for the selection of appropriate levels of sideloading.

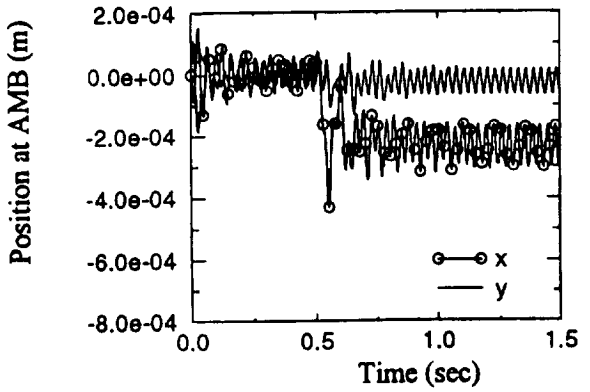

Figure 5.c Rotor Response With AMB Failure
$\Omega = 200\text{rad/sec}, C_L = \frac{D}{3}$
$t_f = 0.5, \alpha = 0$

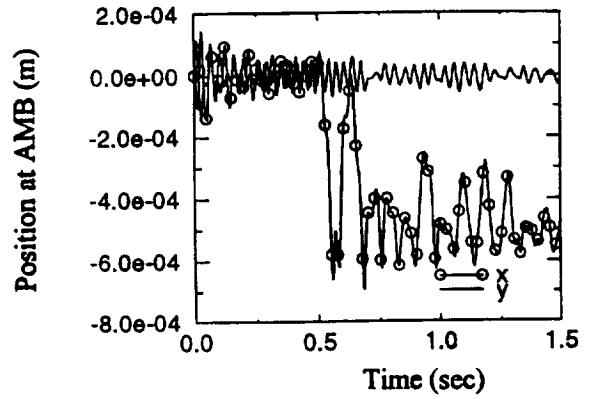

Figure 6.a Rotor Response With AMB Failure
$\Omega = 200\text{rad/sec}, C_L = \frac{2D}{3}$
$t_f = 0.5, \alpha = -100$

ACKNOWLEDGEMENT

This work was supported by the National Aeronautics and Space Administration under Grant No. NAG3-1507. The Government has certain rights in this material. Special appreciation is expressed to Dr. Albert F. Kascak of NASA/Lewis Research Center.

REFERENCES

Gondhalekar, V., and Holmes, R., "Design of a Radial Electromagnetic Bearing for the Vibration Control of a Supercritical Shaft," *Proceedings of the Institution of Mechanical Engineers*, Vol. 198C, No. 16, pp. 235-242.

Habermann, H., and Liard, G., "An Active Magnetic Bearing System," *Tribology Inter-*

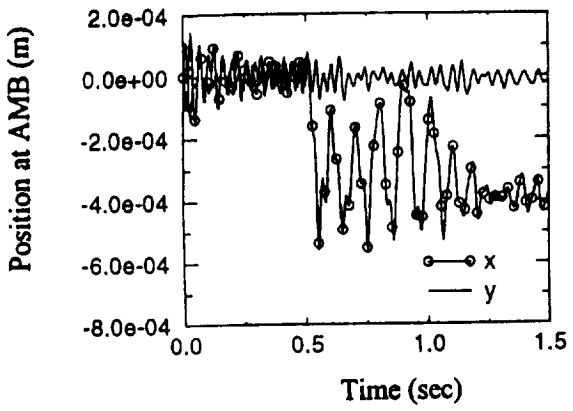

Figure 6.b Rotor Response With AMB Failure
$\Omega = 200\text{rad/sec}, C_L = \frac{D}{2}$
$t_f = 0.5, \alpha = -100$

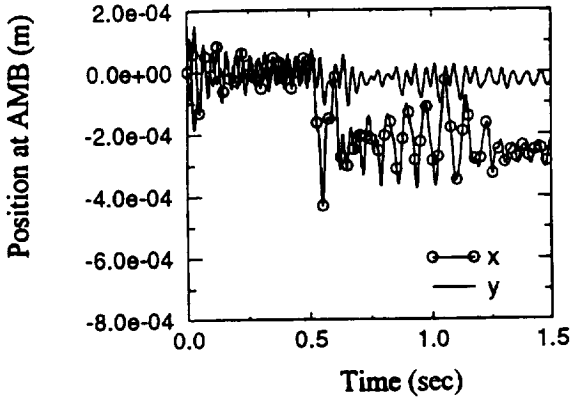

Figure 6.c Rotor Response With AMB Failure
$\Omega = 200\text{rad/sec}, C_L = \frac{D}{3}$
$t_f = 0.5, \alpha = -100$

national, April, 1980, pp. 85–89.

Humphris, R.R., Kelm, R.D., Lewis, D.W., and Allaire, P.E., "Effect of Control Algorithms on Magnetic Journal Properties," *ASME Journal of Engineering for Gas Turbines and Power,* Vol. 108, October, 1986, pp. 624–632.

Ishii, T., Kirk, R.G., "Transient Response Technique Applied To Active Magnetic Bearing Machinery During Rotor Drop," *Rotating Machinery and Vehicle Dynamics,* Vol. 35, 1991, pp. 191–199.

Lewis, David W., "Electro and Permanent Magnet Materials," *Introduction To Magnetic Bearings: A Short Course,* July 27-28, 1993.

Shafai, B., Beale, S., LaRocca, and Cusson,

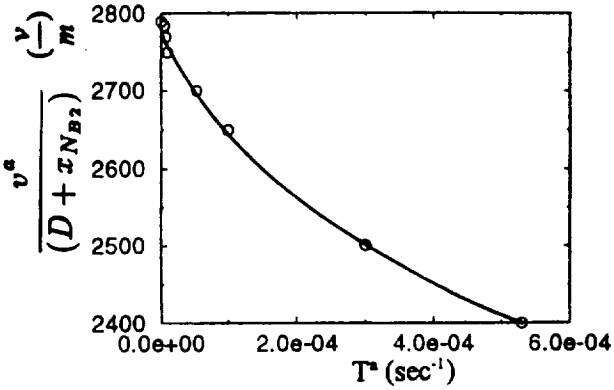

Figure 7 Maximum Sideloading Force as a Function of Power Amplifier Time Constant, τ^a
(for parameters of Table 1)

E., "Magnetic Bearing Control Systems and Adaptive Forced Balancing," *IEEE Control Systems,* Vol. 14, No. 2, pp. 4–13.

APPENDIX LINEAR CURRENT AND POSITION STIFFNESSES

For design purposes, a linearized model for the magnetic bearing forces is needed.

The current stiffnesses are:

$$K_1^i = \frac{\mu_o A k_1^a v_1^{bi} N_T^2}{2D^2} \qquad (7.a)$$

$$K_2^i = \frac{\mu_o A k_2^a v_2^{bi} N_T^2}{2D^2} \qquad (7.b)$$

$$K_3^i = \frac{\mu_o A k_1^a v_1^{bi} N_T^2}{2D^2} \qquad (7.c)$$

$$K_4^i = \frac{\mu_o A k_2^a v_2^{bi} N_T^2}{2D^2} \qquad (7.d)$$

The position stiffnesses are:

$$K_1^P = \frac{\mu_o A (k_1^a v_1^{bi})^2 N_T^2}{2D^3} \qquad (8.a)$$

$$K_2^P = \frac{\mu_o A (k_2^a v_2^{bi})^2 N_T^2}{2D^3} \qquad (8.b)$$

N95- 32693

THE AMERICAN SOCIETY OF MECHANICAL ENGINEERS
345 E. 47th St., New York, N.Y. 10017

95-GT-216

SYNCHRONOUS DYNAMICS OF A COUPLED SHAFT/BEARING/HOUSING SYSTEM WITH AUXILIARY SUPPORT FROM A CLEARANCE BEARING: ANALYSIS AND EXPERIMENT

James L. Lawen, Jr.
Auburn University
Auburn, AL 36849

George T. Flowers
Auburn University
Auburn, AL 36849

ABSTRACT

This study examines the response of a flexible rotor supported by load sharing between linear bearings and an auxiliary clearance bearing. The objective of the work is to develop a better understanding of the dynamical behavior of a magnetic bearing supported rotor system interacting with auxiliary bearings during a critical operating condition. Of particular interest is the effect of coupling between the bearing/housing and shaft vibration on the rotordynamical responses. A simulation model is developed and a number of studies are performed for various parametric configurations. An experimental investigation is also conducted to compare and verify the rotordynamic behavior predicted by the simulation studies. A strategy for reducing sychronous shaft vibration through appropriate design of coupled shaft/bearing/housing vibration modes is identified. The results are presented and discussed.

NOMENCLATURE

C = damping, N-sec/m
K = stiffness, N/m
M_b = auxiliary bearing mass, kg.
M_h = housing mass, kg.
N = total number of modes considered
N_{b1} = node number at leftmost bearing
N_{b2} = node number at rightmost bearing
N_{b3} = node number at auxiliary clearance bearing
$\mathbf{Q}_x$ = rotor modal coordinate vector in X direction
$\mathbf{Q}_y$ = rotor modal coordinate vector in Y direction
t = time, s
X_r = rotor physical coordinate vector in X direction, m
Y_r = rotor physical coordinate vector in Y direction, m
X_b = auxiliary bearing physical coordinate vector in X direction, m
Y_b = auxiliary bearing physical coordinate vector in Y direction, m
X_h = housing physical coordinate vector in X direction, m
Y_h = housing physical coordinate vector in Y direction
Δ = radial clearance in auxiliary bearing, m
$\mathbf{I}_a$ = rotor polar mass inertia matrix, kg-m^2
Ψ = rotor free-free modal rotation matrix
Φ = rotor free-free modal displacement matrix
$\Gamma = \Psi^T \mathbf{I}_a \Psi$
Ω = rotor operating speed, rad/s
ω_n = matrix of rotor free–free natural frequencies, rad/s
ψ = imbalance vector

Subscripts

bx = auxiliary bearing, x-direction
by = auxiliary bearing, y-direction
c = contact
hx = housing, x-direction
hx = housing, y-direction
xr = rightmost bearing, x-direction
xl = leftmost bearing, x-direction
yr = rightmost bearing, y-direction
yl = leftmost bearing, y-direction

Presented at the International Gas Turbine and Aeroengine Congress & Exposition
Houston, Texas - June 5-8, 1995
This paper has been accepted for publication in the Transactions of the ASME
Discussion of it will be accepted at ASME Headquarters until September 30, 1995

INTRODUCTION

In recent years, the use of active magnetic bearings for supporting turbomachinery has been an area of interest for both academic researchers and turbomachinery users in industry. Magnetic bearings provide the potential for significant improvements over other types of rotor support, including elimination of wear and bearing friction-related energy losses as well as a means of actively suppressing rotor vibration. However, their use has been significantly limited due to a number of technical problems. A particular area of concern is the auxiliary bearing, which protects the soft iron core of the magnetic bearing and provides rotor support in case of overload or failure of the magnetic bearing.

Typically, the auxiliary bearings have relatively small clearances so that magnetic bearing rotor/stator contact does not occur during bearing failure or power loss. Due to these small clearances, contact between the rotor system and the auxiliary bearings can occur during standard operation of the magnetic bearings. When this occurs, load sharing between the magnetic bearings and the auxiliary bearings results, and the rotor system interacts with its auxiliary bearings. The dynamics of such an occurrence must be understood in order to properly design the auxiliary bearing system for a magnetic bearing supported rotor.

A number of different bearing types have been suggested as auxiliary bearings. These include bushings, rolling element bearings, and various types of journal bearings. The most commonly considered are rolling element bearings. The major disadvantage associated with using rolling element bearings (or bushings) is the requirement of a clearance between the rotor and the inner race of the bearing, without which many of the advantages associated with using magnetic bearings would be reduced or eliminated. This clearance introduces a nonlinear dynamical feature which may significantly impact the behavior of the rotor.

There are quite a number of studies in the literature concerned with nonlinear rotordynamics. Ehrich (1965 and 1967) studied the rotor/stator interaction with a clearance and found zones of bistable synchronous behavior. Black (1968) also found these bistable interaction zones. Ehrich extended this research by predicting subharmonic behavior (1966 and 1988), superharmonic behavior (1992), and chaotic responses (1991). Bently (1974), Muszynska (1984), and Childs (1979 and 1982) also observed and studied subharmonic responses due to clearance effects.

There is relatively little work available in the open literature that is specifically concerned with the dynamics between the rotor system and the auxiliary bearings. The research that has been performed to date is primarily concerned with the transient behavior of rotor drop on the auxiliary bearings due to power faliure or inoperative magnetic bearings. Two papers with this focus are Gelin et al., (1990) and Ishii and Kirk (1991).

The present work is concerned with developing an understanding of the dynamic behavior of a rotor system supported by load sharing between the linear bearings and an auxiliary bearing with clearance. Of particular interest is the influence of coupled shaft/bearing/housing vibration modes on the rotordynamical behavior of such a system.

SIMULATION MODEL

Figure 1 shows the simulation model used for this investigation. It consists of a flexible rotor supported at both ends by magnetic bearings. A rigid disk with adjustable imbalance is placed at the midpoint of the bearing span. As a simplification, the magnetic bearings are modeled as spring and dashpot systems and interaction with a single auxiliary bearing is considered. The auxiliary bearing was modeled as an antifriction bearing with a clearance and a mass attached to a housing. The housing in turn has a mass, stiffness, and damping. Figure 2 shows the auxiliary bearing model used in the simulation.

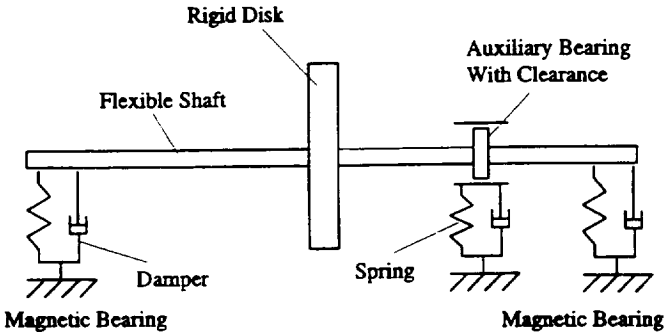

Figure 1 Schematic Diagram of Simulation Model

The rotor is modelled using the free–free bending mode shapes and natural frequencies obtained through finite element analysis. The finite element code uses 19 stations and the first four modes (two rigid body and two flexible modes) are included in the simulation model.

Using these simplifications, the equations of motion for the system can be written as follows:

$$\ddot{\mathbf{Q}}_x + \Omega\Gamma\dot{\mathbf{Q}}_y + \omega_n^2\mathbf{Q}_x + \Phi^T(F_{x,lin} + F_{x,nl})$$

$$= \Phi^T F_{x,imb}, \quad (1.a)$$

$$\ddot{\mathbf{Q}}_y - \Omega\Gamma\dot{\mathbf{Q}}_x + \omega_n^2 \mathbf{Q}_y + \Phi^T(F_{y,lin} + F_{y,nl}) = \Phi^T F_{y,imb}, \quad (1.b)$$

$$M_b\ddot{X}_b + \frac{C_{bx}}{\Omega}(\dot{X}_b - \dot{X}_h) + K_{bx}(X_b - X_h) = F_{x,nl}, \quad (1.c)$$

$$M_b\ddot{Y}_b + \frac{C_{by}}{\Omega}(\dot{Y}_b - \dot{Y}_h) + K_{by}(Y_b - Y_h) = F_{y,nl}, \quad (1.d)$$

$$M_h\ddot{X}_h + (\frac{C_{bx}}{\Omega} + \frac{C_{hx}}{\Omega})\dot{X}_h + (K_{bx} + K_{hx})X_h = C_{bx}\dot{X}_b + K_{bx}X_b, \quad (1.e)$$

$$M_h\ddot{Y}_h + (\frac{C_{by}}{\Omega} + \frac{C_{hy}}{\Omega})\dot{Y}_h + (K_{by} + K_{hy})Y_h = \frac{C_{by}}{\Omega}\dot{Y}_b + K_{by}Y_b, \quad (1.f)$$

where

$$\mathbf{F}_{x,lin} = \Phi_{N_{b1}}(K_{xl}\mathbf{Q}_x + \frac{C_{xl}}{\Omega}\dot{\mathbf{Q}}_x) + \Phi_{N_{b2}}(K_{xr}\mathbf{Q}_x + \frac{C_{xr}}{\Omega}\dot{\mathbf{Q}}_x)$$

$$\mathbf{F}_{y,lin} = \Phi_{N_{b1}}(K_{yl}\mathbf{Q}_y + \frac{C_{yl}}{\Omega}\dot{\mathbf{Q}}_y) + \Phi_{N_{b2}}(K_{yr}\mathbf{Q}_y + \frac{C_{yr}}{\Omega}\dot{\mathbf{Q}}_y)$$

$$\mathbf{F}_{x,imb} = \psi\Omega^2 cos\Omega t,$$

$$\mathbf{F}_{y,imb} = \psi\Omega^2 sin\Omega t,$$

$$\mathbf{F}_{x,nl} = \phi K_c(\delta - \Delta)(\frac{\Phi\mathbf{Q}_x - X_b}{\delta})$$

$$\mathbf{F}_{y,nl} = \phi K_{cont}(\delta - \Delta)(\frac{\Phi\mathbf{Q}_y - Y_b}{\delta})$$

$$\delta = \sqrt{(\Phi\mathbf{Q}_x - X_b)^2 + (\Phi\mathbf{Q}_y - Y_b)^2},$$

$$\phi = 1 \; if \; \delta > \Delta$$

$$0 \; otherwise$$

$$\mathbf{Q}_x = \Phi^{-1}\mathbf{X}_r,$$

$$\mathbf{Q}_y = \Phi^{-1}\mathbf{Y}_r,$$

with

$$\mathbf{X}_r = \{X_{r1}, X_{r2}, \ldots, X_{rm}\}^T,$$

$$\mathbf{Y}_r = \{Y_{r1}, Y_{r2}, \ldots, Y_{rm}\}^T.$$

(m = total number of nodes)

The physical displacements of the rotor at the auxiliary bearing or magnetic bearing locations can be obtained using the following coordinate transformation:

$$X_{rk} = \sum_{i=1}^{N} \Phi_{ki} Q_{xi}, \qquad (k = N_{b1}, N_{b2}, N_{b3})$$

$$Y_{rk} = \sum_{i=1}^{N} \Phi_{ki} Q_{yi},$$

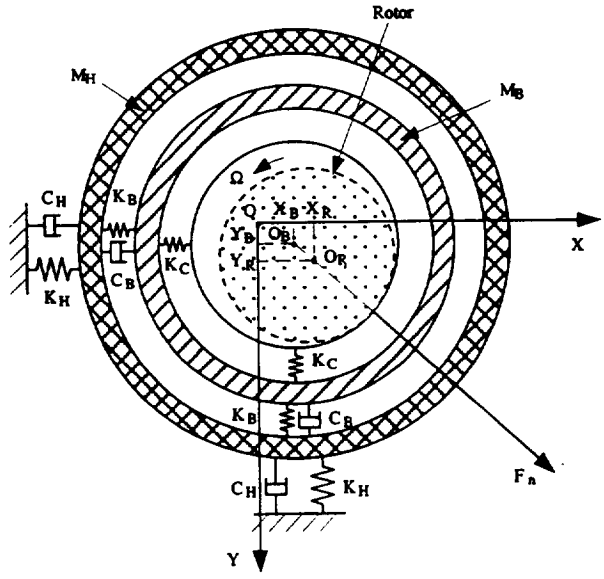

Figure 2 Auxiliary Bearing Model

EXPERIMENTAL MODEL

Experimental tests were performed in order to validate the behavior predicted by the simulation model and to gain some insight into the dynamical responses that are to be expected. A schematic diagram of the rotor test rig that was used in the experimental work is shown in Figure 3.

The rotor used in this study has two basic components: a flexible shaft and an auxiliary clearance bearing. The shaft is made of steel and is 0.374 inches in diameter and 18.0 inches in length. It is supported at 1.0 inch from the right end by ball bearings suspended in a frame by four springs and at 1.0 inch from the left end by a bushing with a tight clearance. These supports

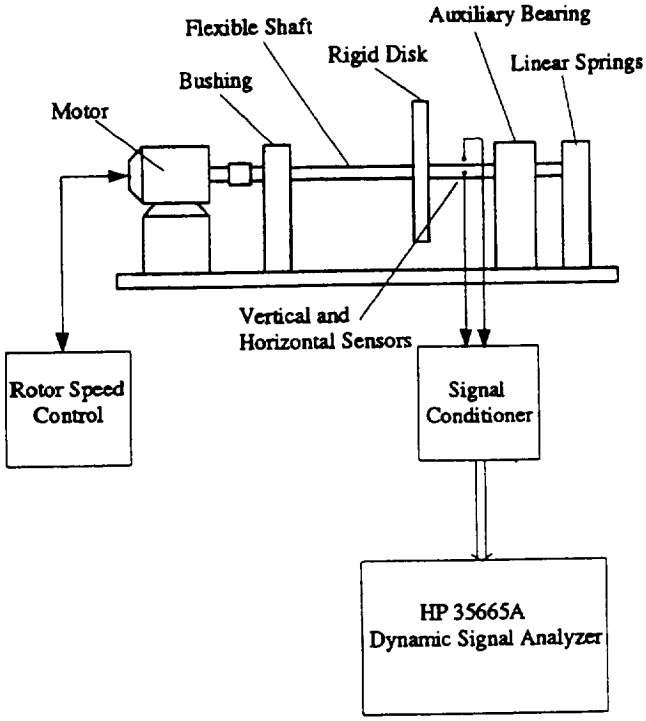

Figure 3 Experimental Model

represent the magnetic bearings. The stiffness of the left support is 17511 N/m (101.5 lb/in) for both the horizontal and vertical directions. It is used to somewhat isolate the rotor from the effects of the flexible coupling which attaches the rotor to the motor and to enforce low amplitude vibration at this location to protect the motor. The stiffness of the right support, for both horizontal and vertical directions, is 2539 N/m (14.5 lb/in). This lower stiffness allows for significant vibration of the rotor in the speed range of the motor. A rigid disk with an adjustable imbalance is placed at the midpoint of the bearing span. The auxiliary clearance bearing/housing consists of a bushing suspended in a frame by four springs (Figure 4). It is situated at the right end of the rotor. The clearance is adjustable by changing the bushing. The auxiliary bearing/housing stiffnesses are varied by interchanging the springs.

The rotor is driven by an adjustable speed motor with feedback speed controller. Shaft vibration is measured using eddy current proximity displacement sensors fixed so as to measure displacement in the vertical and horizontal directions. The displacement signals were recorded and analyzed with a signal analyzer.

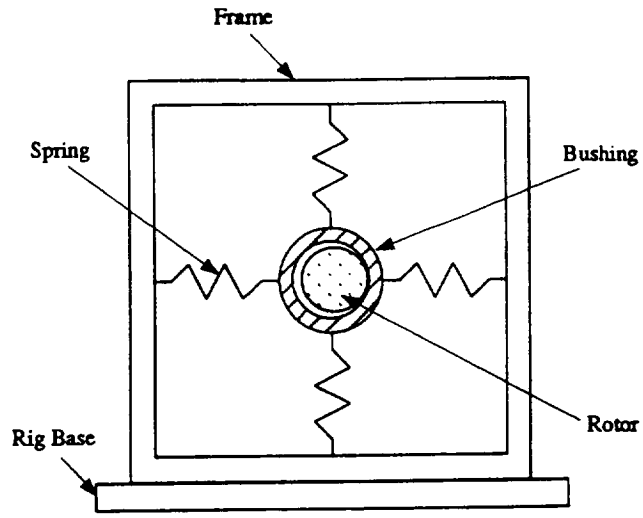

Figure 4 Auxiliary Clearance Bearing

DISCUSSION

A series of parallel studies were conducted using the simulation and experimental models discussed in the preceding sections. The following discussion is aimed at comparing the predictions of the simulation model with experimentally observed responses, with the objective of obtaining insight into the behavior of flexible rotor system dynamics due to load sharing between the magnetic bearings and an auxiliary bearing.

Using the data from measurements and calculations, the stiffness, damping, and mass characteristics of the experimental rotor system were identified. The imbalance configuration consists of 3.0 x 10^{-6} kg-m located at the left end of the rotor shaft (from the flexible coupling to the electric motor) and a variable imbalance located on the rigid disk. Linear, hysteretic, and coulomb friction damping models were considered. The support damping appears to result principally from hysteresis. If synchronous vibration is assumed, this results in a damping coefficient scaled by the rotor speed. The numerical values are given in Table 1.

The governing parameters for an auxiliary bearing are stiffness, mass, damping, clearance, and axial location. The axial location generally is fixed by other considerations, such as space requirements and the need to be close to the magnetic bearing to better protect it. This study focusses on the remaining design parameters. For the system studied, significant nonsynchronous vibration occured only for the 2ω component and for a limited rotor speed range. Figure 5 illustrates the observed behavior for various imbalance values. The amplitudes are quite small and, interestingly, virtually independent of imbalance. The remainder of this discussion will focus on the synchronous response amplitudes.

Parameter	Value	Units
K_b	471	N/m
K_h	$1.8x10^7$	N/m
K_c	87,557	N/m
K_{lx}, K_{ly}	17,510	N/m
K_{rx}, K_{ry}	2,539	N/m
C_{lx}, C_{ly}	1,000	N/m
C_{rx}, C_{ry}	500	N/m
C_{ly}, C_{ly}	1,000	N/m
C_{ry}, C_{ry}	500	N/m
C_{bx}, C_{by}	2,000	N/m
C_{hx}, C_{hy}	0	N/m
M_b	0.033	kg
M_h	0.296	kg
ψ_1	3.0×10^{-6}	kg-m
ψ_{10}	2.5×10^{-5}	kg-m
Δ	$5.0x10^{-5}$	m

Table 1 Simulation Model Parameters

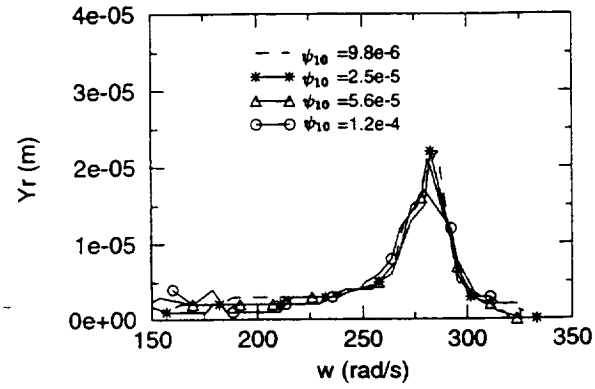

Figure 5 Experimental Results for 2ω Component

The simulation responses discussed below were determined from a single-term harmonic balance analysis that was numerically implemented and verified at selected points using direct numerical integration of the governing equations of motion. The harmonic balance procedure is described by Nayfeh and Mook (1979). Figures 6.a - 6.e show the response amplitudes predicted from the simulation study for the parameters of Table 1. Figures 7.a - 7.c show some corresponding experimental results. The rotor speed range extends to above the second critical speed, with the first critical speed primarily a rotational mode and the second critical speed primarily a translational mode.

Figures 6.a presents simulation results for varying auxiliary bearing stiffness and Figure 7.a shows the corresponding experimental values. There is relatively good agreement between the actual and predicted responses except for the peak values which are very sensitive to damping. At lower rotor speeds, the stiffness effect from the auxiliary bearing tends to dominate and serves to increase the effective lower critical speed. At higher rotor speeds, the inertial effects of the bearing tend to dominate and the added mass serves to lower the effective second critical speed. This effect is balanced somewhat for higher stiffnesses (as is expected), as can be seen for the case with K_b=2,625 N/m. The damping added to the system from the auxiliary bearing serves to attenuate the peak response amplitudes for both critical speeds. The response amplitudes between the two response peaks are affected little by the auxiliary bearing, with the rotor and bearing/housing vibrations tending to decouple for response amplitudes below the clearance. Above the second critical speed, the presence of the auxiliary bearing serves to reduce the response amplitudes for the remainder of the plot. For this region, there is significant coupling between the rotor/bearing/housing vibration and the response amplitudes are below the clearance for speeds greater than about 550 rad/sec. The rotor speed ranges for which coupling of the rotor/bearing/housing vibration will occur depend upon the phase of the combined system response, as described by Black (1968). For the purposes of this study, K_b=471 N/m is chosen as a reasonable value and variations of other parameters are performed with this auxiliary bearing stiffness.

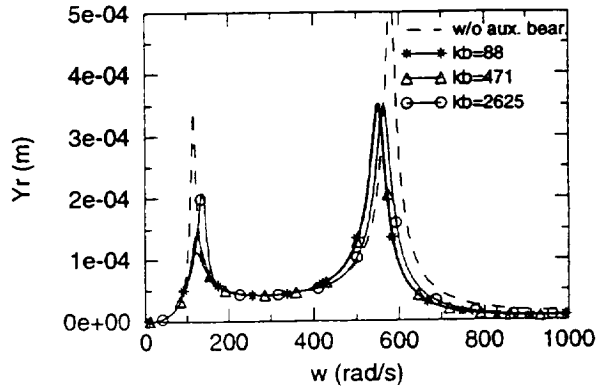

Figure 6.a Simulation Results for Varying Auxiliary Bearing Stiffness

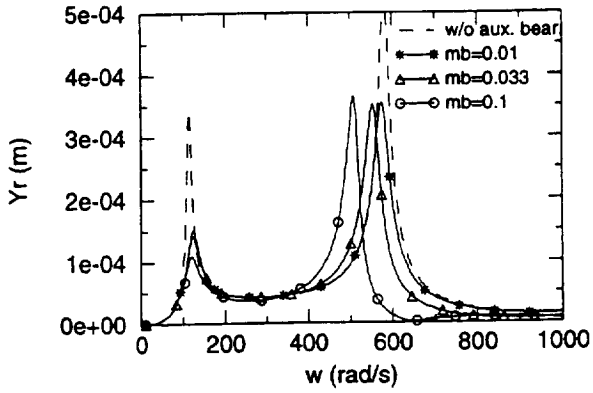

Figure 6.b Simulation Results for Varying Auxiliary Bearing Mass

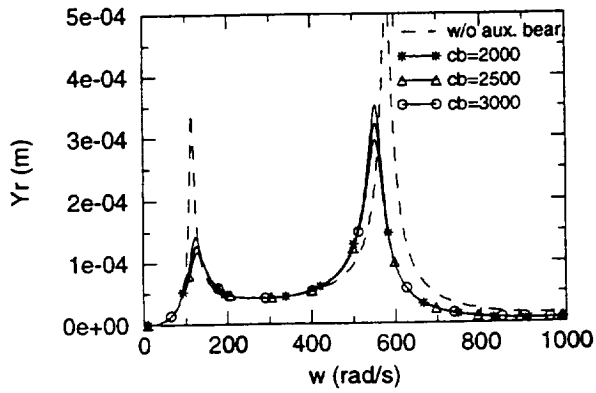

Figure 6.c Simulation Results for Varying Auxiliary Bearing Damping

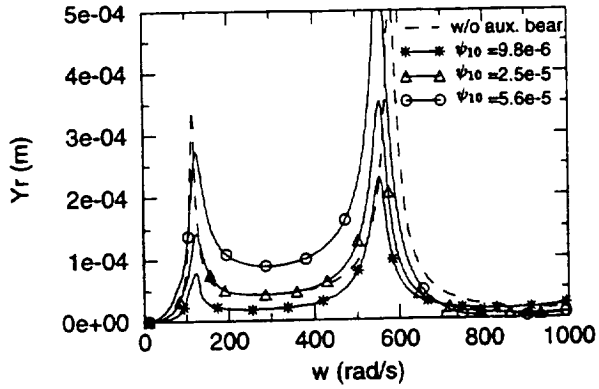

Figure 6.d Simulation Results for Varying Imbalance

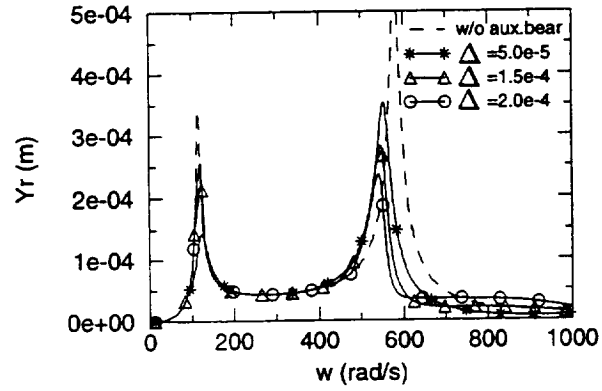

Figure 6.e Simulation Results for Varying Auxiliary Bearing Clearance

Figures 6.b shows the predicted rotor response for the parameters of Table 1 with the bearing mass varied. These results show that the more massive bearing/housing configurations can result in much lower amplitude rotor responses. In fact, for sufficiently high mass values, the response amplitude is dramatically reduced for the rotor speed range from about 600 rad/sec to about 780 rad/sec where it merges with other amplitude response curves. Figure 6.c shows the effect of auxiliary bearing damping on the rotor response. While the response amplitudes remain relatively unchanged for the majority of rotor speeds, higher damping does serve to significantly reduce the rotor response amplitudes through the critical speeds. Damping also effects the phase characteristics of the combined rotor/bearing/housing system and changes the rotor speed ranges for which coupled responses occur. Figures 6.d and 7.b show the rotor response for the parameters of Table 1 with the imbalance varied. As expected, the response amplitudes increase with increasing imbalance. Figures 6.e and 7.c show the rotor response amplitudes with the auxiliary bearing clearance varied. As the clearance increases, the dynamics of the combined rotor/bearing/housing vibration tend to decouple over a wider speed range between the two critical speeds. Again, such behavior is expected from the analysis work for a rotor operating in an annular clearance performed by Black (1968).

Close examination of the above results reveals a very interesting trend. Turbomachine are designed to operate at rotor speeds between the various system critical speeds so as to minimize synchronous

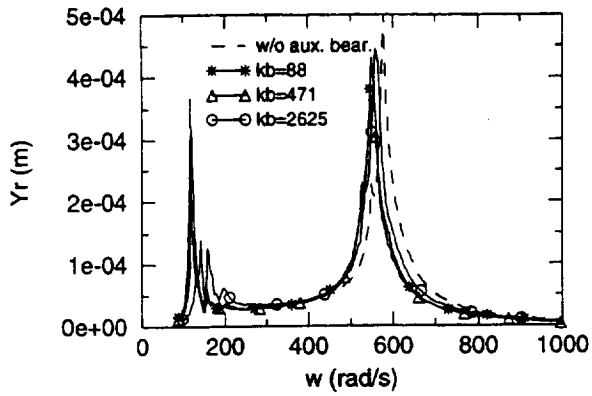

Figure 7.a Experimental Results for Varying Auxiliary Bearing Stiffness

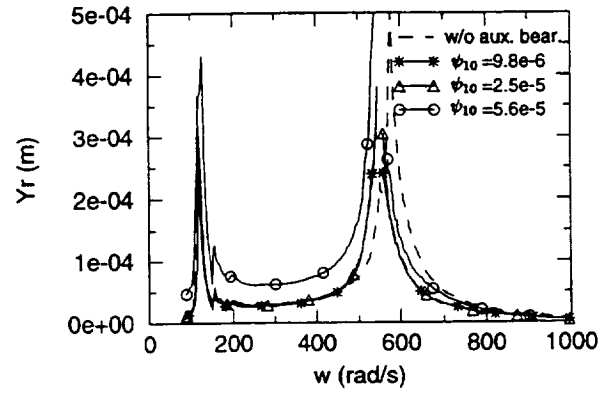

Figure 7.b Experimental Results for Varying Imbalance

response amplitudes. For the present system, the lowest amplitude responses (for operation above the second critical speed) occur for the auxiliary bearing configurations where there is the largest decrease of the second effective critical speed, which is due to a coupling of rotor/stator/housing vibration. While not really suprising, this result indicates an interesting strategy for the design of auxiliary support using clearance bearings. Selection of combined shaft/auxiliary bearing/housing vibration characteristics such that the effective critical speeds nearest the operating speed (directly above and below) shift away from it should result in lower amplitude rotor vibration and provide the best opportunity to protect the magnetic bearing. However, the phase characteristics of the combined system must be such that vibration coupling occurs

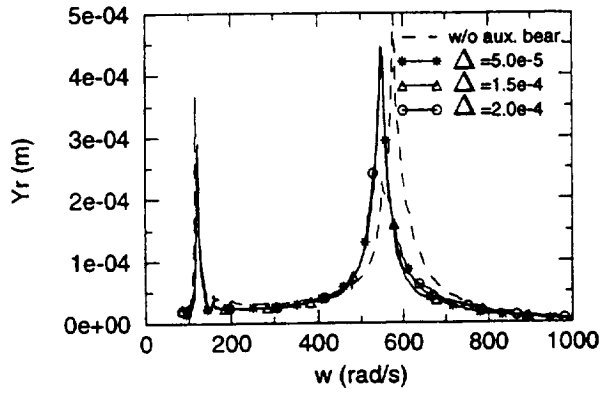

Figure 7.c Experimental Results for Varying Auxiliary Bearing Clearance

and care must be taken to ensure that this is the case if the maximum benefit is to be derived from the auxiliary bearing.

CONCLUSIONS

A study of the dynamical behavior of a flexible rotor supported by linear bearings (representing a set of magnetic bearings) and an auxiliary bearing with clearance has been presented. Parallel simulation and experimental studies have been performed for a variety of parametric configurations. The influence of bearing mass, stiffness, damping, clearance, and imbalance were examined. It was observed that the dynamic behavior of a rotor interacting with an auxiliary bearing depends very strongly on the structural parameters of the auxiliary bearing and associated housing. Appropriate selection of these parameters is critical if acceptable vibration characteristics are to be obtained for such systems. In general, one must carefully consider the influence of housing/bearing dynamics and how to best take advantage of favorable coupled modes of vibration in the development of auxiliary bearing designs.

ACKNOWLEDGEMENT

This work was supported by NASA under Grant No. NGT-70312 and Grant No. NAG3-1507. The Government has certain rights in this material. Appreciation is expressed to S.C. Sinha, S.G. Ryan and A.F. Kascak for their advice and assistance in this research effort.

REFERENCES

Bently, D. E., 1974, "Forced Subrotative Speed Dynamic Action of Rotating Machinery," ASME Paper No. 74-PET-16.

Black, H. F., 1968, "Interaction of a Whirling Rotor With a Vibrating Stator Across a Clearance Annulus," *Journal Mechanical Engineering Science*, Vol. 10, No 1, pp. 1–12.

Childs, D. W., 1979, "Rub-Induced Parametric Excitation in Rotors," *ASME Journal of Mechanical Design*, Vol. 101, pp. 640–644.

Childs, D. W., 1982, "Fractional-Frequency Rotor Motion Due to Nonsymmetirc Clearance Effects," *ASME Journal of Engineering for Power*, Vol. 104, pp. 533–541.

Ehrich, F. F., 1965, "Bistable Vibrations of Rotors in Bearing Clearance," ASME Paper 65–WA/MD–1.

Ehrich, F. F., 1988, "High Order Subharmonic Response of High Speed Rotors in Bearing Clearance," *ASME Journal of Vibration, Acoustics, Stress, and Reliability in Design*, Vol. 110, pp. 9–16.

Ehrich, F. F., 1992, "Observatons of Subcritical Superharmonic and Chaotic Response in Rotordynamics," *ASME Journal of Vibration and Acoustics*, Vol. 114, pp. 93–100.

Ehrich, F. F., 1991, "Some Observatons of Chaotic Vibration Phenonema in High-speed Rotordynamics," *ASME Journal of Vibration, Acoustics, Stress, and Reliability in Design*, Vol. 113, pp. 50–57.

Ehrich, F. F., 1966, "Subharmonic Vibration of Rotors in a Bearing Clearance," ASME Paper 66-MD-1.

Ehrich, F. F., and O'Conner, J. J., 1967, "Stator Whirl with Rotors in Bearing Clearance," *ASME Journal of Engineering for Industry*, August, pp. 381–390.

Gelin, Al, Pugnet, J. M., and Hagopina, J. D., 1990, "Dynamic Behavior of Flexible Rotors with Active Magnetic Bearings of Safety Auxiliary Bearings," *Proceedings of 3rd International Conference on Rotordynamics*, Lyon, France, pp. 503–508.

Ishii, T., and Kirk, R. G., 1991, "Transient Response Technique Applied to Active Magnetic Bearing Machinery During Rotor Drop," *DE-Vol. 35, Rotating Machinery and Vehicle Dynamics, ASME*, pp. 191–199.

Muszynska, A., 1984, "Partial Lateral Rotor to Stator Rubs," IMechE Paper No. C281/84.

Nayfeh, A.H., and Mook, D.T., 1979, Nonlinear Oscillations, John Wiley and Sons, pp. 59–61.

Ryan, S.G., 1991, "Limit Cycle Vibrations in Turbomachinery," NASA Technical Paper 3181.